

One-Dimensional Carbon Nanostructures: Low-Temperature Chemical Vapor Synthesis and Applications

Yao Ma, Nianjun Yang and Xin Jiang

Abstract Chemical vapor deposition (CVD) is a powerful method to synthesize various carbon nanostructures (e.g., carbon nanotubes). A conventional CVD process has to be carried out at the temperatures over 600 °C. To extend the applications of carbon nanostructures, for example in the semiconductor industry, low-temperature synthesis processes are thus always pursued. In this chapter we review the CVD growth of carbon nanostructures at low temperatures (<450 °C). These growth processes are discussed in detail with respect to the applied catalyst system, carbon source, reaction atmosphere, catalyst faces, morphology control as well as unique structural characteristics of grown products. For the low-temperature CVD growth, catalytic reaction occurring on the low index faces of a metal catalyst is a crucial issue, and the growth is rate-limited by surface diffusion. Instead of the classical Vapor-Liquid-Solid (VLS) growth mechanism, the growth mechanism at low temperatures is interpreted with a novel Vapor-Facet-Solid (VFS) mechanism. Due to their unique features, the synthesized carbon nanostructures are promising to be applied for interconnects in large-scale integrated circuits, field emission, microwave adsorption, and as the anode material of lithium ion secondary battery, etc.

Keywords Carbon nanostructure • CVD • Low temperature • Catalyst • Growth mechanism

1 Introduction

One dimensional (1D) carbon nanostructures (CNs) usually refer to the structures, which feature large aspect ratios and small diameters (<100 nm). The typical 1D CNs, carbon nanofibers (CNFs) entered people's consciousness initially as harmful byproducts during metal-catalytic synthesis processes, and thus in the early studies researches aimed to inhibit the formation of CNFs. An interesting turning occurred

Y. Ma · N. Yang · X. Jiang (✉)
Institute of Materials Engineering, University of Siegen,
Paul-Bonatz Str. 9-11, 57076 Siegen, Germany
e-mail: xin.jiang@uni-siegen.de

in 1991 due to the discovery of a special CNF by Iijima [1], which is constructed by cylindrical graphitic sheets. It was named as carbon nanotube (CNT). Researchers are then attracted by distinct properties of the CNTs such as extremely high strength, aspect ratio, specific surface area, as well as unique optical and electrical features [2–4]. Since then many scientists worldwide have focused on exploring new techniques to synthesize CNTs, because of their extensive application potentials.

Three main techniques have been developed to grow CNTs, including catalytic CVD, arc-discharge [5, 6], and laser-ablation technique [7, 8]. Among them the catalytic CVD strategy has the distinct advantages due to its large-scale production ability of CNTs at relative low temperatures and low cost. Hence it is the most popular technique. In a catalytic CVD growth process, the catalysts (e.g., small-sized metal particles) are firstly heated in a reaction chamber. Carbon containing source gas is then introduced, a series of chemical and physical processes start and lead to the deposition of carbon and finally the formation of CNTs on the catalysts.

In the research fields of catalytic CVD growth of CNTs, lots of other types of carbon nanostructures besides cylindrical CNTs have been synthesized. In term of morphology, they can be sorted to straight nanofiber [9], nanohelix [10], nanocoil [11], nanocone [12], and nanobelt [13], etc. According to structural characteristics (the size and orientation of graphitic sheets constructing the CNs), they feature tubular [14, 15], herringbone-like [16–18], bamboo-like [19–22], and amorphous nature [23].

The morphologies, microstructures and properties of CNs prepared in CVD process are determined by both the catalysts preparation and subsequent growth conditions. In this context, it has been found that transition metals, such as Fe, Co, Ni and their alloys are the effective catalysts for the growth of CNs, and the transition metals with different compositions and morphologies can lead to CNs with different morphologies. As a result, the preparation of effective catalysts has become a significant step for the synthesis of CNs. Numerous methods have been thus employed to prepare these catalysts, including sol-gel method [24, 25], co-reduction of precursors [26, 27], impregnation and incubation [28, 29], ion-exchange-precipitation [30], reverse micelle method [31], thermal decomposition of carbonyl complexes [32, 33], and metal organic chemical vapor deposition (MOCVD) [29].

Different gases, including CH_4 , CO, C_2H_2 , C_2H_4 , benzene were used as carbon source for the growth of CNs. The effects of flow rate, temperature, and additional ingredient such as oxygen and sulfur in reaction atmosphere have been investigated.

Special configuration of the synthesis equipments has been also explored. By using microwave assisted chemical vapor deposition (MWCVD) technique, Fe catalysts were used to catalytically synthesize carbon nanocone [12], carbon nanohelix [34], carbon nanotip [35, 36], and carbon nanobelt [37]. Aligned CNs arrays were often synthesized in electric field induced by bias in the system [38, 39]. Nowadays, the research of CNs is keeping more on the development of their precise morphology control and their extensive applications.

To date, the upsurge of the research about CNFs, CNTs and other CNs has lasted for two decades. During this period the investigations were not only focused on their synthetic methods and applications, the attention was also devoted to the essence of the CVD growth processes. In the commonly accepted growth

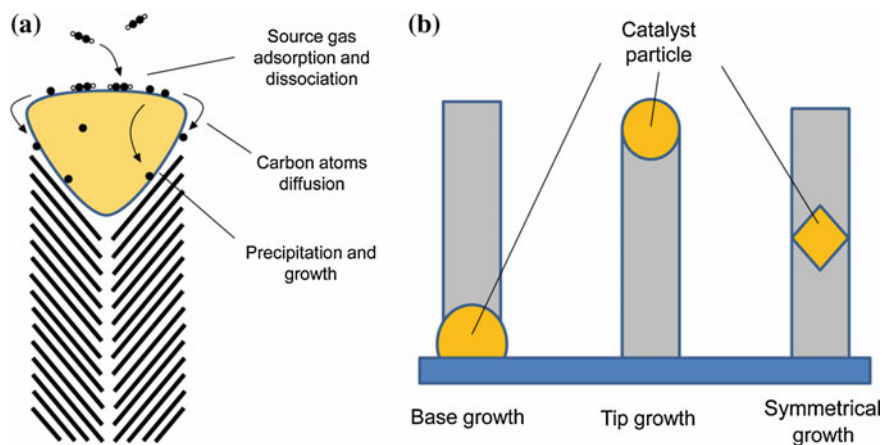


Fig. 1 Sketch of the nanofiber growth: **a** VLS mechanism, **b** three different growth modes

mechanism, carbon dissolves into the catalyst and CNs grow due to the precipitation of excess carbon on the surface of the catalyst (in most cases, it is a metal particle). This idea originates from the vapor-liquid-solid (VLS) mechanism suggested by Wagner et al. to explain the growth of single crystal Si wire [40, 41]. In particular, it is now frequently used to interpret the catalytic CVD growth of 1D CNs. As shown in Fig. 1a, the basic concept is as following: (i) adsorption and dissociation of carbon containing gas on the surface of the catalyst, (ii) diffusion of carbon atoms through the catalyst, and (iii) precipitation of carbon from saturated catalyst particles to form 1D CNs. In this model, the catalyst forms a liquid droplet and preferentially adsorbs the growth species from the surrounding vapor, and the solid carbon wire grows from this supersaturated eutectic liquid.

In the VLS model, the catalyst is the core of the whole reaction system because all important processes progress on or within the catalyst. Any change of the catalyst will be finally reflected on the grown nanostructure. The size of the catalyst (e.g., metal particle) is treated as the determining factor for the diameter of the grown CNs; whilst the crystalline orientation plays a critical role in the determination of CNTs chirality [42, 43]. As for the preparation methods of the catalyst, they influence as well the catalysts' size and their dispersion on the surface of the support and thereby their catalytic properties [44, 45]. For example, the interactions between the metal catalyst and the surface of the support were found to determine the growth mode [14, 46, 47]. Weak interactions yield a tip-growth whereas strong interactions lead to a base-growth. Moreover, distinct activity for hydrocarbon molecule dissociation or carbon atom extrusion on different surfaces of the catalyst [48, 49] is believed to be responsible for a symmetrical growth, as schematically shown in Fig. 1b. These experimental facts suggest that the geometric features of the catalyst play important roles in the growth of CNs. However, in previous studies the effect of the geometric shape of the catalyst on the growth of CNs did not attract enough attention because this concept is beyond the basic framework of the VLS mechanism and certain shaped catalyst is not necessary for a VLS process.

On the other hand, according to the VLS mechanism, the peculiar ability of transition metals (e.g., Fe, Co and Ni) to catalyze CNs' formation is greatly linked to their catalytic activities in the decomposition of hydrocarbons and their allowance of extremely rapid carbon atomic diffusion (both through and over their surfaces). This ability depends strongly on the growth temperature applied. At low temperatures the catalytic reactions on metal surface are quite different from those at high temperatures. For example, carbon solubility and diffusion coefficient decrease significantly [50, 51]. Therefore, in practical most of the CVD growth processes were carried out at the temperatures higher than 600 °C.

However, the attempt to synthesize CNs through CVD growth at low temperatures has not been given up. Firstly, the carbon containing source gases applied in the CVD growth processes (e.g., CH₄, C₂H₂, C₂H₄) are normally explosive. A process at lower temperatures is much safer. The low-temperature CVD process also simplifies remarkably the equipment and reduces consequently the cost. Secondly, the CVD processes are often accompanied by the decomposition of hydrocarbons and coking. The process at lower temperatures mitigates the harmful deposition from the wall of a reaction chamber as well as gas channels. Finally and the most importantly, the growth at low temperatures is of great benefit to a lot of applications when the substrate material cannot withstand a high-temperature process. For example, to apply CNFs in semiconductor industry, the CVD process has to be compatible with the CMOS technology. It means the CVD temperatures must remain below 400–450 °C to avoid mechanical deterioration [52].

Therefore, in this chapter we focus only on the CVD processes which employ temperatures below 450 °C. We summarize recent progress and achievements about the low-temperature CVD growth of 1D CNs, and then discuss the unique growth mechanisms for the growth of these 1D CNs. Some example applications of these 1D CNs are shown as well.

2 Synthesis of 1D Carbon Nanostructure at Low Temperatures

So far, the low-temperature synthesis of CNs has been achieved successfully by applying normal catalytic thermal CVD methods. In a typical thermal CVD process, the growth progresses in a reaction chamber (e.g., quartz tube) which is connected to a gas supplying system. Metal catalyst is pre-placed in the chamber or brought in by a carrier gas during the process. Once the chamber is heated up to reach desired temperature, carbon containing source gas (e.g., C₂H₂, CH₄) is introduced. Consequently CNs grow with the aid of the catalyst. Different temperatures, from 195 to 450 °C, have been used for the growth of various CNs, including CNTs, amorphous CNFs, carbon nanocoils (CNCs), carbon nanohelices (CNHs), carbon nanosheets (CNSs), and branched CNs. Table 1 lists some representative growth conditions and related CNs achieved.

Table 1 The reported low-temperature thermal CVD processes

Catalyst	Carbon source	Temperature (°C)	Flow	Product	Reference
Ni, Cu–Ni, Co–Ni, Fe–Ni	CH ₄	450		CNF	[53]
Ferrocene	C ₂ H ₂ C ₈ H ₁₀	450	Ar, H ₂ as carrier	CNT	[54]
Fe ₂ Co	C ₂ H ₂ /CO ₂	400		CNT	[55]
Fe–Co–Ni	C ₂ H ₂	400	C ₂ H ₂ 10 sccm N ₂ 100 sccm	MWCNT	[56]
Fe–Co	C ₂ H ₂	400	C ₂ H ₂ 50 sccm N ₂ 250 sccm	CNT	[57]
Ni–Fe	C ₂ H ₂	400		CNT CNF	[58, 59]
Cu–Ni	C ₂ H ₂	400	C ₂ H ₂ 3 sccm He 12 sccm	CNF	[60]
Ni	C ₂ H ₂	400		CNT	[61]
Co	Alcohol	400		SWCNT	[52, 62]
Cu	C ₂ H ₂	350	Ar 20 sccm H ₂ 10 sccm C ₂ H ₂ 5/10 sccm NH ₃ 0/10 sccm	CNF	[63]
Fe	C ₂ H ₂	350		CNF	[64]
Ni ₃ C	Nickel(II) acetylacetonate	300	H ₂ 200 sccm	CNF	[65]
Ni _{0.67} Fe _{0.33}	C ₂ H ₂	300	C ₂ H ₂ 0.5 sccm H ₂ 50 sccm	CNT	[66]
Cu	C ₂ H ₂	250–350		2-, 3-, 6-, 8-branched CNF	[67]
Cu	C ₂ H ₂	250		CNH CNF	[68, 69]
Cu	C ₂ H ₂	250		CNS	[70]
Cu	C ₂ H ₂	195		CNH	[71]

To get a deep insight into the characteristics as well as the mechanisms of low-temperature growth, we discuss in the following sessions these processes in detail from the aspects of catalyst system, catalyst evolution, the effect of gas composition on the growth as well as the morphology control on the growth products.

2.1 Types of Catalysts

It is similar to those conventional high-temperature CVD growths, transition metals such as Fe, Co, Ni and their alloys are often used as the catalysts for the low-temperature growth of CNs. Comparing with pure metals, their alloys show

higher catalytic activity. When other experimental parameters remain unchanged, the catalyst from their alloy triggers a growth at lower temperatures, or causes higher growth rates of CNs [56, 66]. However, tri-metallic catalysts do not show any advantage over bimetallic ones [56, 57]. For example, Chiang and Sankaran [66] tested different Fe–Ni alloyed catalysts and gave an optimal composition of approximately 67 % Ni and 33 % Fe.

Cu has been used as the catalyst for the growth of CNs. Notably, in a conventional high-temperature CVD process Cu is not an effective catalyst, because carbon hardly dissolves (diffuses) in Cu [51]. In contrast, in the low-temperature cases Cu is quite attractive to aid the synthesis of various CNs. For example, by applying a Cu catalyst the growth of CNs was achieved at a temperature as low as 195 °C [71]. It is 100 °C lower than the temperatures for those processes based on Fe, Co, Ni catalysts. Therefore the Cu catalyzed growth of CNs is believed to be a typical case of the low-temperature CVD growth. It might correspond to a unique growth mechanism, different from the VLS mechanism.

Besides the chemical composition of the catalyst, its size is critical for the growth of CNs as well. To effectively catalyze the growth of a nanostructure, the catalysts (e.g., in a form of nanoparticle or nanonetwork) must be well dispersed on a substrate. The size and the dispersion of the catalyst directly decide the dimension and the amount of as-grown CNs. A simple and often used method for the catalyst preparation is a coating-anneal route [57, 61]. Briefly, a metal film with a few to tens of nanometers in thickness is firstly coated on a substrate. In the following annealing the metal film at high temperatures splits and converges the metal film into dispersive nanoparticles. As an example, SEM images of one 20 nm thick Cu film before and after annealing are shown in Fig. 2a and b, respectively. In this way one can use a target with a certain composition during sputter coating process to get the catalyst with a required composition [57, 58]. The size of the catalyst is possible to be adjusted by changing the thicknesses of the metal film and annealing times/temperatures. Other methods are also available for the preparation of these catalysts, for example, sol-gel [67], co-precipitation [55], thermal decomposition [56], arc plasma jet evaporation methods [64], and thermolysis of various complex precursors in hot surfactant solutions [72]. The as-prepared metal catalysts usually have however random near-spherical or polyhedron shape.

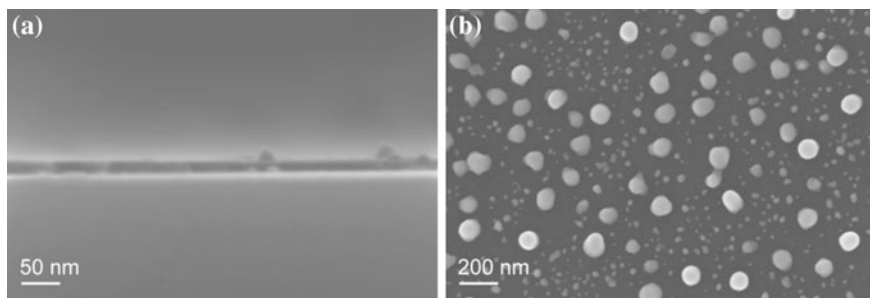


Fig. 2 SEM images of **a** cross section of a 20 nm Cu film coated on Si substrate and **b** dispersive Cu nanoparticles after annealing

The pre-treatment of the catalysts influences their catalytic activities. For example, Shyu et al. reported that by pre-treating the Ni or Fe–Ni catalyst with low-concentrated carbon containing source gas, the growth of CNFs was promoted in the following CVD processes. In contrast, if the catalyst was pre-treated with reductive H_2 , the CVD growth was depressed [59]. The reason of such a promotion was believed to be the formation of Ni–C or Fe–Ni–C alloy.

2.2 Catalyst Faceting

The growth of CNFs is always accompanied by tremendous shape change of the catalyst. For instance, the Cu catalyst are always faceted with regular shapes after the CNs growth, the majority of which have a rhombic projection. Detailed investigations indicate that the Cu catalyst undergoes a shape change from an irregular to a regular faceted form during the CNs growth. Moreover, their shapes have considerable effects on the final cross-sections of CNs. Based on systemic TEM observations as well as accompanying selected area electron diffraction (SAED) indexes performed by Xia et al., the Cu catalyst (e.g., particles) in as-grown nanostructures can be sorted to three kinds of basic highly symmetric polyhedrons, namely octahedron, triangular prism and tetrahedron, as shown in Fig. 3 [73]. Octahedron catalyst particle is in the left column (Fig. 3a, d, f, i) and triangular prism catalyst in the middle column (Fig. 3b, e, g, j). From upper to bottom row they are the TEM images of a straight nanofiber, the TEM image of a helical nanofiber, the sketch of a catalyst particle, and the projection of a catalyst particle along Cu $\langle 110 \rangle$ zone axis, respectively. In the right column (Fig. 3c, h, k), it shows Cu catalyst with the shape of tetrahedron. From upper to bottom row they are the TEM images of straight nanofiber, the sketch of catalyst particle, and the projection of catalyst particle along Cu $\langle 110 \rangle$ zone axis, respectively. One can see that for these grown nanofibers, regardless of the morphology of the nanofiber and the shape of the catalyst, Cu particles are all encompassed by low-index faces and CNFs always attaches on Cu $\{111\}$ faces. In the TEM image as well as HRTEM images of Fig. 4a, b, one can see the grown carbon product is connected to Cu catalyst with a quite flat interface. When the focus is on the grown carbon product, the HRTEM image shows discontinuous near-parallel fragments, indicating amorphous nature of grown CNFs, as seen in Fig. 4c [73].

The catalyst faceting appears on Fe and Ni based catalyst along with the CNFs growth as well [64, 65]. Figure 5a shows a TEM image of a CNF grown at 350 °C where Fe catalyst is encapsulated in the fiber. The Fe particle has a polygonal projection and features the $\{110\}$ face as the growth front [64]. Figure 5b shows a typical TEM image of a symmetrical CNF grown at 350 °C when a Ni catalyst particle is applied. One can see an approximate rhombus projection in the TEM

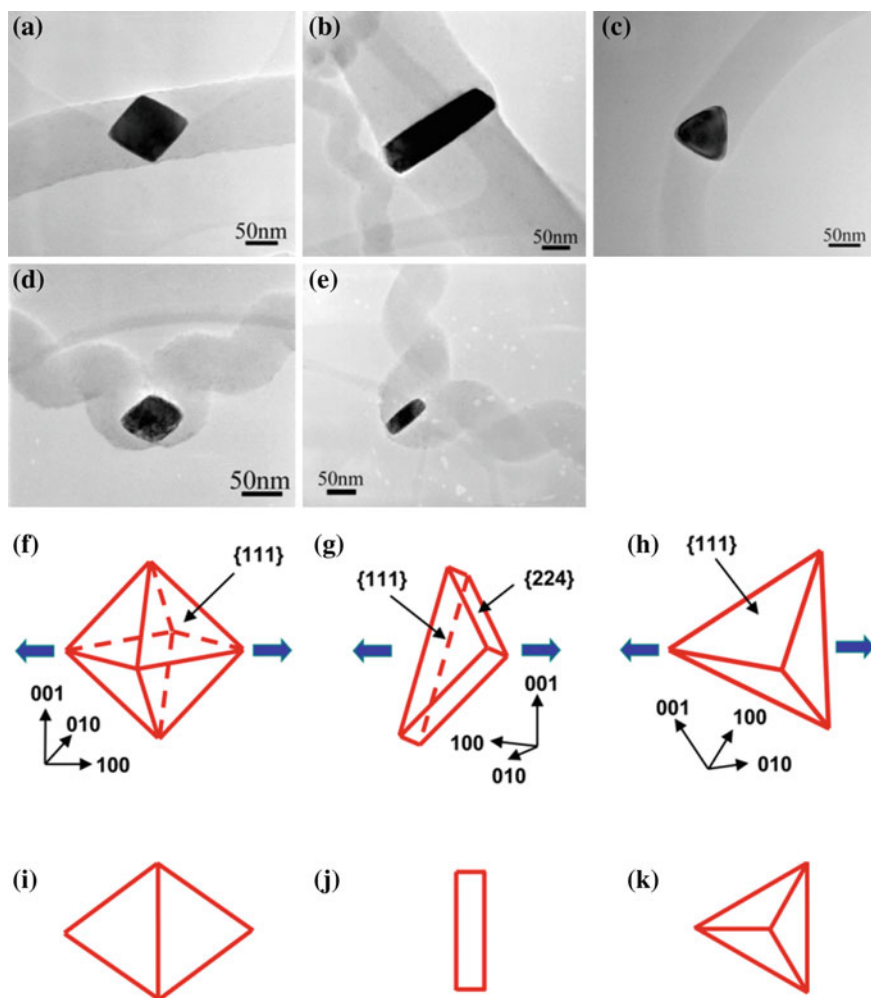


Fig. 3 a–e TEM images of different morphologies of nanostructures obtained along Cu $\langle 110 \rangle$ zone axis. f–h Three kinds of catalyst polyhedrons: octahedron, triangular prism and tetrahedron, respectively. i–k The respective projections of the polyhedrons (f–h) obtained along Cu $\langle 110 \rangle$ zone axis [73]

image. For the Ni_3C assisted growth at a quite low temperature of 300 °C, Yu et al. performed HRTEM observation and stated that the growth of CNFs is initiated from the {001} planes of the Ni_3C particles which exhibit a regular shape [57].

As a result of faceting, the shape of the catalyst evolves until specific stable crystalline faces expose. In particular, the low index faces tend to appear. It indicates that these faces play important roles in the growth of CNFs. Some critical

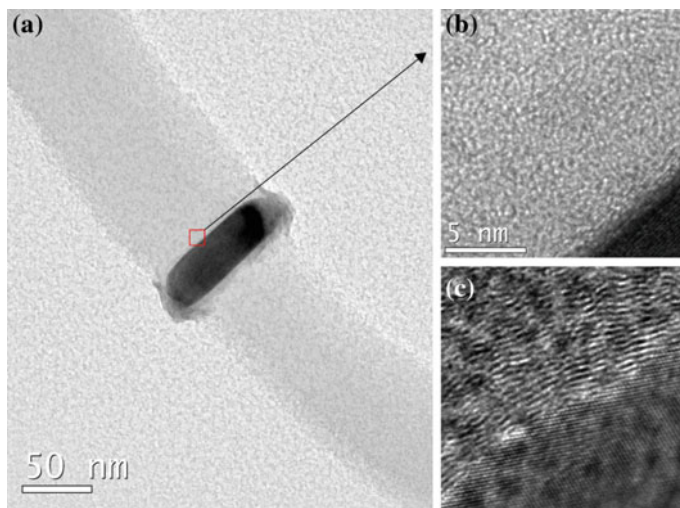


Fig. 4 The enlarged TEM images of a CNF. **a** The TEM image on Cu [112] zone axis. The fiber is grown on the catalyst along Cu $\langle 111 \rangle$ crystal direction. **b** HRTEM images of the areas indicated with *red square* in (a). It shows a flat interface between grown carbon and the catalyst. **c** HRTEM image focusing on the grown carbon product [73]

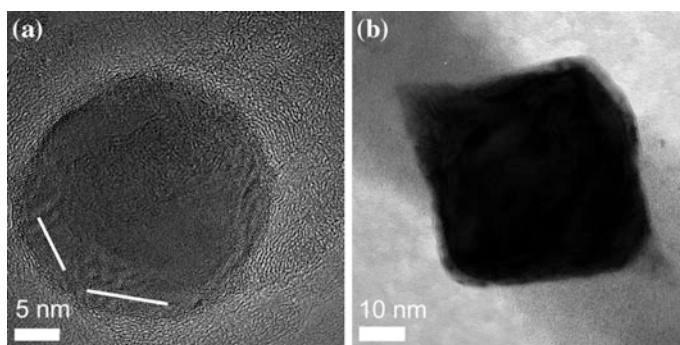


Fig. 5 **a** TEM image of the tip of a CNF. The *dark particle* is Fe catalyst. The *bright lines* mark the (110) plane of the Fe catalyst. **b** TEM image of a symmetrical grown CNF. The *black spot* is Ni catalyst particle

processes such as surface reactions may progress on certain indexed metal planes, e.g., the {111} faces of a Cu particle. Unfortunately, so far relatively limited attention has been paid to the effect of the geometric features of the catalyst on the low-temperature CVD growth of CNs.

2.3 Gas Composition

In the CVD growth of CNs, the carbon feedstock relies on carbon containing source gases. For the conventional high-temperature growth, many carbon containing gases are applicable, such as CH_4 , C_2H_2 , C_2H_4 , CO , benzene etc. [74–78]. On the contrary, only a few carbon sources have been successfully applied in the low-temperature CVD growth up to now. As summarized in Table 1, most of the successful processes were achieved with C_2H_2 . Some researchers replaced C_2H_2 with other carbon sources (e.g., C_2H_4 , CH_4 , CO) as controlled experiments, but only negative results were obtained [58, 71], revealing a high selectivity of carbon sources for the low-temperature CVD growth of CNs. Two hypotheses might be workable for the high activity of C_2H_2 . Firstly, at low temperatures, the cleavage of C_2H_2 to generate atomic carbon is easier, in comparison with other carbon containing molecules [79]. Therefore the growth with C_2H_2 can happen at lower temperatures. Another possibility is the unique structure of C_2H_2 allows it adsorbing on the catalyst in a property way and participating in special catalytic surface reactions.

Besides carbon sources, unreactive gases have been also introduced on purpose during the growth process, such as N_2 , Ar, He and sometimes H_2 . Although they do not contribute to the construction of CNs directly, their roles are somehow critical. For example, in some experimental settings they work as the carrier gas to bring the catalyst into the reaction chamber [54]. Moreover, except few special processes which require ultra-high vacuum (UHV) condition [52, 62], most of the low-temperature CVD growth can progress in a broad pressure range (even in atmospheric pressure [64, 67, 71]). Therefore, the growth is often accompanied with cocking and the generation of a large amount of organic byproducts. The unreactive gas dilutes the reactive atmosphere [56, 57, 60] and then prevent or alleviate the harmful deposition on the wall of the reaction chamber and gas channels. Meanwhile, the reaction byproducts can be taken away if the unreactive gas passes the reaction chamber as a constant flow.

It has been reported that a little amount of water (~ 100 ppm) in the reaction atmosphere promoted the CNT growth in a high-temperature CVD process [80, 81]. Based on this idea, a method so-called water assisted CVD was developed [82, 83]. The truth of the promotion is that the mild oxidizer such as water helps to prevent amorphous carbon deposition on the surface of the catalyst [80, 81], thus the poison of the catalyst is efficiently avoided. This method was further extended to applying other oxygen containing gas, for example O_2 [84] and CO_2 [85, 86]. Researches confirmed that NH_3 has the ability to etch amorphous carbon [78, 87, 88]. However, for the low-temperature CVD growth using additional etching gases seems to be unnecessary. For most of reported low-temperature processes, only carbon containing source gases and unreactive gases were applied. It implies that amorphous carbon does not become an obstacle to the growth of CNs at low temperatures. A possible explanation is that at low temperatures the diffusion of carbon atoms and related molecules is mainly through the surface of catalyst, therefore the surface of

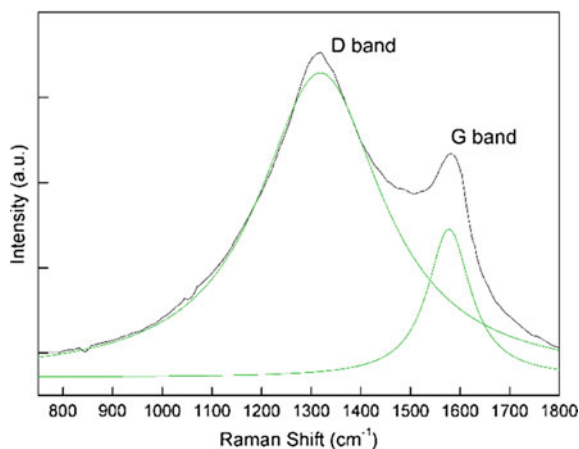
the catalyst is always scoured by moving reaction products. In other words, the surface of the catalyst is always fresh and active. Recently we found that some gases (e.g., HCl) depressed the growth of CNs at low temperatures, as they eliminate specific active faces on the catalyst. For example, when a little amount of HCl is introduced into the reaction atmosphere of a Cu assisted CVD process, the Cu {110} face enlarges while the Cu{111} face shrinks. It is due to the strong interaction between HCl and the Cu{110} face [89, 90]. As the CNF only grows on the Cu{111} face, consequently the as-grown nanofiber becomes thinner and the total amount of growth product reduces [67].

2.4 Structural Characteristic of the Carbon Nanostructure Synthesized at Low-Temperature

Most of CNs synthesized using the low-temperature CVD processes have amorphous natures. From their HTREM images one can see that these CNs feature usually discontinuous fragments rather than integral graphitic sheets [64, 65, 67, 73]. The example TEM images are shown in Fig. 4. Consequently, their Raman spectra often show a D peak with a high intensity, indicating their poor crystallinity, as seen in Fig. 6. It should be pointed out that although a lot of literatures involving the low-temperature CVD growth used ‘CNT’ to define their fiber-like products, they did not give clear evidence (e.g., TEM) to prove these claimed structures. Therefore it is doubtable to classify those products into CNT in standard sense, which normally indicates a highly ordered graphitic tubular nanostructure.

In a systematic investigation, we performed CVD growths under atmospheric pressure of C_2H_2 with the assistance of Fe, Co, Ni, and Cu nanopowder catalysts, respectively. The process temperatures were set between 250 and 350 °C. Regardless of the catalyst, all the synthesized CNs contain considerable hydrogen. Normally,

Fig. 6 Raman spectrum of a CNF which was synthesized via a CVD process at 350 °C. Ni and C_2H_2 were used as the catalyst and carbon source, respectively



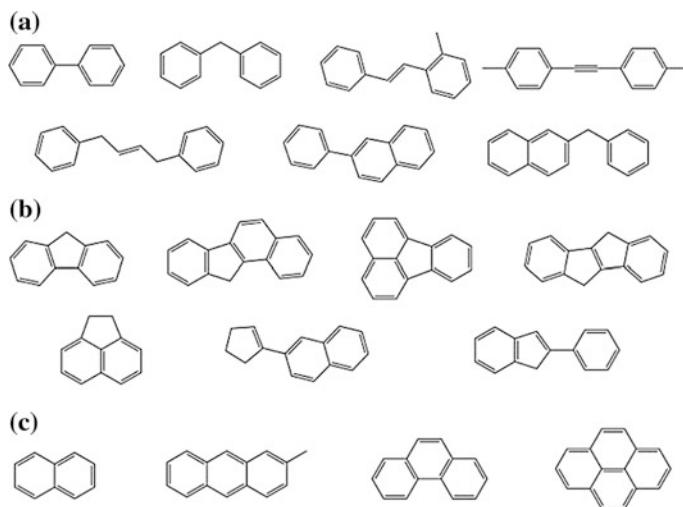


Fig. 7 Molecular fragments presented in the as-grown CNFs, which were identified from the TD-GC/MS method [64, 91]. **a** connected by short carbon chain, **b** connected by five-membered ring, **c** form fused six-membered ring

the lower the growth temperature is, the higher percentage of hydrogen is contained in as-grown CNs [71]. In a typical case, the Cu assisted growth progressing at 250 °C, the product contains about half hydrogen in atomic percentage. Therefore the CNs synthesized via low-temperature CVD processes shows more or less polymer natures. Furthermore, by means of thermal desorption-gas chromatography/mass spectrometry (TD-GC/MS) technique, more detailed structural characteristics of synthesized CNs were revealed. The synthesized CNs were firstly heated up to release fragments (thermal desorption), and then these evaporated species were injected into GC for separation and final identification by MS. No matter the catalyst is Fe, Co, Ni or Cu, the measurements always reveal a series of planar benzene derivatives, such as diphenyl, phenanthrene, anthracene, benz(a)azulene, 9-Methylene-fluorene, etc., as shown in Fig. 7. They are believed to be the intermediate products or the fragments of the CNs. Consequently it can be concluded that benzene rings act as the fundamental structural units and form other planar molecules. The paths to construct other molecules are a connection by short carbon chains, resulting in the formation of five-membered rings as well as fused six-membered rings [64].

3 Morphology Control

The morphology of nanomaterials is of great significance for their electronic, electrochemical, optical, magnetic, and catalytic features as well as their applications [92–97]. Therefore considerable effort was devoted to the morphology control

during synthesizing nanostructures [98–100]. In terms of CNs, by applying high-temperature CVD processes, various CNs have been synthesized, including CNTs [101], nanocones [12], Y-junctions [102, 103], nanocoils [104], fullerenes [105], etc. They are actually quite useful since specific CNs are preferred for some special applications [106–108]. However, comparing with the results achieved on metal nanocrystals [93, 95, 97], metal oxides, and semiconductors [92, 98], the morphology control of CNs is far less precise. Actually if a fact that highly ordered crystalline lattice does not exist inside CNs exists, it is easy to conclude that most shape-control methods developed for nanocrystals are not applicable over CNs. Fortunately, the low-temperature CVD growth grants more chances to deal with the precise shape-control of CNs.

Xia et al. [69] investigated Cu assisted low-temperature CVD growth and reported a relationship between the size of the catalyst and the morphology of as-grown CNFs, namely a size effect. They suggested there is a critical size of the catalyst to divide the growth of two kinds of CNFs, as shown in Fig. 8. Straight CNFs are formed with larger catalysts while helical CNFs are formed with smaller ones. The critical value is ~ 70 nm for the octahedron shaped catalysts and ~ 110 nm for the triangular prism ones [69]. Therefore it is highly possible to synthesize CNFs with desired morphology by use of certain sized and shaped catalysts.

We further developed a method to control the growth and get CNs with more complex shapes, so-named multi-branched CNs. The core idea of this method is to tailor the shape of the catalyst which decides the morphology of grown CNs [13, 109, 110]. It is notable that metallic catalysts are intrinsically symmetric and always tend to expose favorable low index facets in thermodynamic equilibrium status [111]. In this context a precise shape control of CNs can be achieved via intentionally tailoring the geometric features of the catalyst and exposing its specific catalytic-active facets.

Figure 9 shows 4 different branched CNs [67]. By means of carrying out the CVD growth with assistance of Cu catalyst at 250, 275 and 350 °C, we obtained 2-, 3-, and 6-branched CNs respectively. In these nanostructures, Cu nanocrystal works as a node and carbon branches grow on $\{111\}$ or $\{001\}$ faces of Cu nanoparticle, depending on the process temperatures. In general, the outer surface of Cu

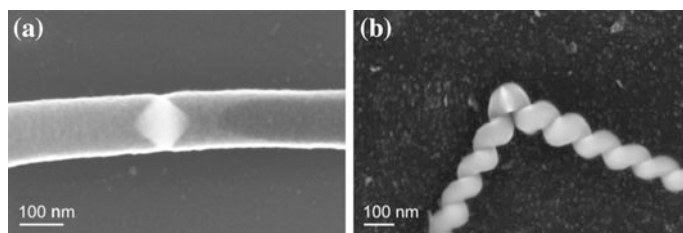


Fig. 8 SEM image of two kinds of CNFs synthesized at 250 °C: **a** a straight nanofiber, **b** a helix nanofiber

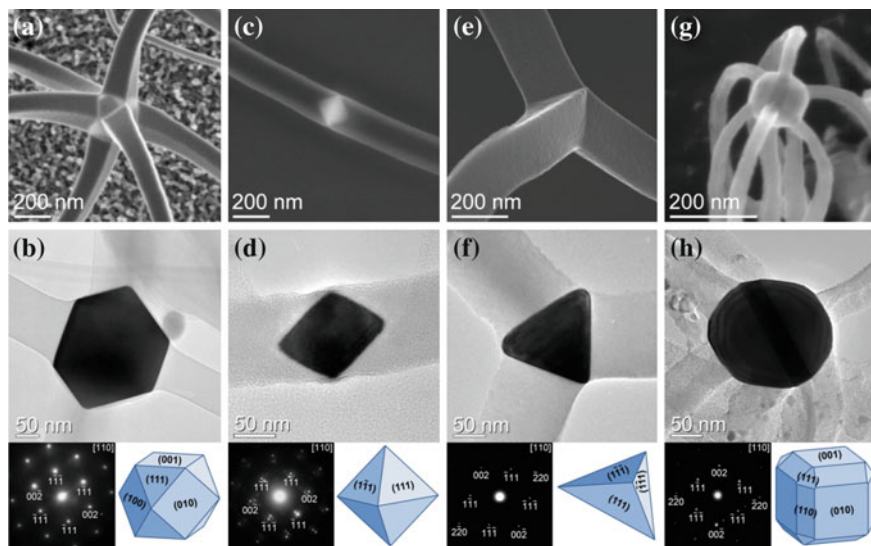


Fig. 9 **a** SEM image and **b** TEM image, electron diffraction pattern, catalyst particle sketch of a 6-branched CN prepared at 350 °C. **c** SEM image and **d** TEM image, electron diffraction pattern, catalyst particle sketch of a 2-branched CN prepared at 250 °C. **e** SEM image and **f** TEM image, electron diffraction pattern, catalyst particle sketch of a 3-branched CN prepared at 275 °C. **g** SEM image and **h** TEM image, electron diffraction pattern, catalyst particle sketch of a 8-branched CN prepared at 250 °C with additional HCl in the reaction atmosphere [67]

nanoparticle is a combination of {001}, {110} and {111} facets [111]. Corresponding to different process temperatures, the Cu particles show unique equilibrium shapes and faceted surface with specific index distribution. The facet distribution was further tailored via adding a little amount of HCl in the CVD chamber. It changed the ratios of {001}, {110} and {111} faces, resulting in the growth of 8-branched CNs. In terms of the carbon branches in these CNs, their numbers and stretching directions follow the intrinsic symmetry of Cu nanocrystals. Their lengths depend on the growth duration. Their diameters correlate to both the size of Cu particles and the distribution of catalysis-active facets on Cu particles. All these features are tailorable via changing experimental parameters.

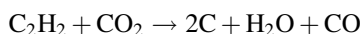
4 Mechanism of Low-Temperature Thermal CVD Growth

With respect to the mechanism of the low-temperature CVD growth of CNs, the core issue is the approach to convert carbon containing gas into solid carbon structures. In this context we have to explain not only the generation of carbon feedstock but also the route for carbon transportation, for example carbon diffusion

through/on the catalyst. For high-temperature CVD growth, the classical VLS model has given appropriate explanation on above issues, see Sect. 1. Unfortunately, the VLS mechanism cannot be used to interpret the low-temperature cases, if the fact that the carbon solubility and diffusion coefficient decrease significantly with the reduction of the growth temperature is noticed [50, 112, 113]. In particular, for the typical Cu assisted growth which produces polymer-like CNs, it completely excludes the possibility of VLS approach, because neither carbon nor hydrocarbon molecules dissolves (diffuses) in the Cu catalyst [51]. Therefore a new model is necessary to interpret the mechanism of the low-temperature thermal CVD growth of CNs on these metal catalysts.

4.1 Fundamental Reactions

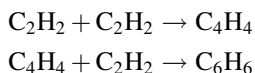
Since at lower temperatures a direct dissociation of hydrocarbons is more difficult, various reaction paths have been proposed to interpret carbon feedstock during the CVD growth. For example, Magrez et al. [55] proposed an oxidative dehydrogenation reaction to explain the growth of CNTs below 500 °C



This approach is however only applicable for those processes with additional CO₂ introduction into the reaction atmosphere. For most CVD processes which progress in pure C₂H₂, the reactions should follow fully different routes.

Fortunately, the interaction of hydrocarbons such as acetylene with the surface of low-index metal single-crystals under ultra-high vacuum (UHV) conditions has been investigated for a long time. These efforts contribute well to a fundamental understanding of important catalytic surface processes, unravel fundamental mechanisms in heterogeneous catalysis, and identify important surface intermediates in practical reactions. Taking the Cu/C₂H₂ system as an example, the adsorption and surface reactions of acetylene on Cu low-index surfaces ({110}, {001}, and {111}) under UHV conditions have been widely investigated both theoretically and experimentally [114–118]. The coupling of acetylene on Cu surface has been demonstrated, which forms benzene (C₆H₆) on Cu{001} [119], Cu {110} [120], Cu{111} facets [121] and cyclooctatetraene (COT, C₈H₈) on Cu {111} facet [121]. In these investigations, no coverage threshold for the onset of the cyclization reactions was observed on any Cu facets, implying high adsorbate mobility [119–121]. It was also confirmed that the reaction pathways of Cu catalytic reactions in atmospheric pressure of acetylene were in good agreement with the model under UHV conditions [71, 121]. Another aspect that should be taken into consideration is the fact that a graphene sheet matches a Cu{111} facet very well (both are in *D*_{6h} symmetry and the mismatch of lattice parameter is about 2 %), which can dramatically increase the interactions between a Cu{111} facet and a graphene sheet as well as its derivatives. Therefore, the fundamental reaction in the

Cu assisted CVD growth is proposed to be the trimerization of C_2H_2 on the low-index Cu surface. It was achieved in following path [71, 119–121]



Based on these reaction pathways various planar benzene derivatives (oligomers) are formed. The oligomers are further polymerized to construct larger planar fragments as well as CNs eventually.

In terms of other catalyst system, above approach is also workable. Previous research carried out under UHV conditions showed that the adsorption of C_2H_2 on a Fe surface induces the formation of various hydrocarbons such as methane, ethane, butane and benzene, but no C3 and C5 products. It was always assumed that the former were created via hydrogen abstraction, C–C bond breaking, dimerization, and trimerization of C2 entities [122]. The literatures have shown that that adsorbed C_2H_2 can dehydrogenize or couple on Ni surface to form a series of hydrocarbon molecules [123–126]. Among these surface reactions, oligomerization [127, 128], e.g., the cyclic trimerization of C_2H_2 on Ni(111) face to form benzene [124], and following polymerization which generates polymer-like products [129] are notable. They can provide fundamental structural units for the construction of CNs.

4.2 Feedstock Transportation/Diffusion Route

For the growth a nanostructure such as a nanofiber, a stable transportation path between reaction products' generation and precipitation/extrusion has to be established on the catalyst. Otherwise the reaction products will simply accumulate on the surface of the catalyst and prevent any further surface reactions as well as the further growth. Therefore the feedstock transportation on the catalyst is a critical issue.

Based on the experimental data of bi- and tri-metallic catalysts assisted low-temperature thermal CVD growth, Pitkänen et al. performed simulation and got very low activation energies for the CVD growth of CNs. It was suggested that the carbon diffusion is the rate-limiting step rather than the hydrocarbon cracking [57]. Yazyev et al. calculated a barrier of 0.39 eV for the diffusion of adsorbed carbon atoms on the Ni(111) surface, which agreed with the activation energy obtained from the experimental CNT growth process. Therefore surface diffusion is the rate-limiting step for low-temperature CVD growth of CNs [130–132].

Certain diffusion mechanisms on base of carbon diffusion on the surface of the catalyst have been thus proposed for CVD growth of 1D CNs [133–139], especially for the low-temperature CVD growth process, which is a low energy path for the growth of CNTs [130]. The surface diffusion channel is also believed to be the reason of increased catalytic activity of nanoparticle alloys at low temperatures [66]. Meanwhile, the calculation of adsorbed atomic carbon diffusion on Cu

surfaces featured surprisingly low barriers of 0.07 eV. The energy barrier of atomic carbon diffusion on Cu surfaces is also lower than that on Ni [131]. Thus the relative low-temperature Cu assisted CVD growth of CNs is reasonable, as listed in Table 1.

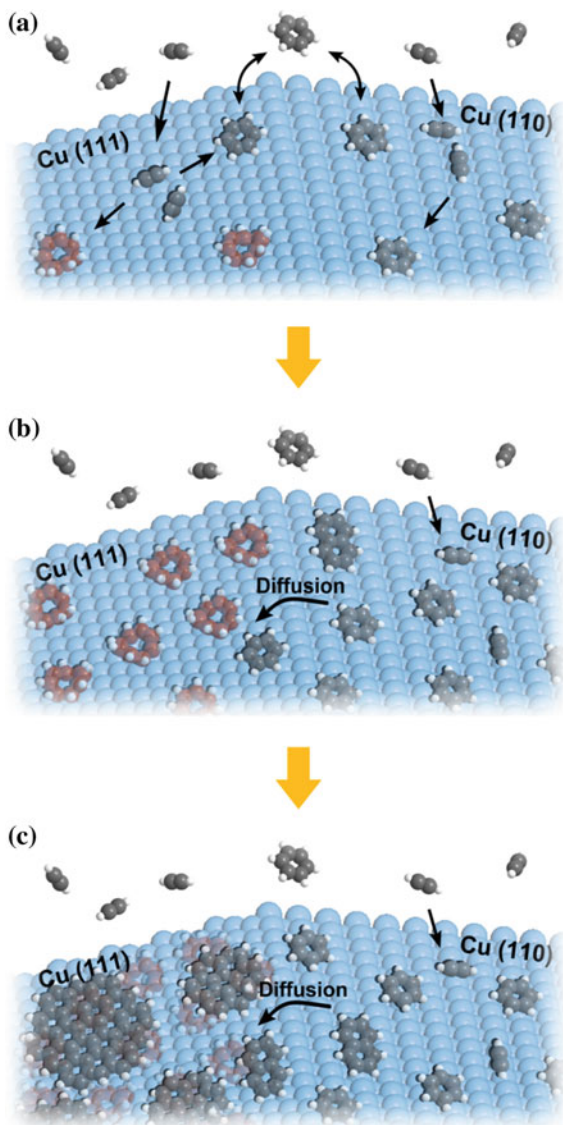
4.3 VFS Mechanism

Based on the characteristics of low-temperature thermal CVD growth of CNs, we describe a 3-step mechanism to interpret the polymers/CNFs growth on the surface of the metal catalyst, as schematically shown in Fig. 10.

Here we still take the Cu/C₂H₂ system as an example. In first step, at a typical growth temperature of 250 °C which is much lower than the melting point, Cu/CuO particles remain in a solid phase. They initiate from irregular shapes. Along with the reduction process on the Cu surface, the acetylene molecules adsorb on the Cu surface and start to couple and polymerize with each other as well as induce Cu surface to reconstruct. The interaction and reaction route of acetylene molecular with Cu facets differ according to the index of facets. On Cu{001} and Cu{110} facets, the coupling reaction products, oligomers such as benzene and its derivatives, have high mobility; while on Cu{111} facet, in addition to benzene formation, small amount of COT forms and it is immobilized at the surface of the Cu catalyst when the temperature is lower than approximately 300 °C [121]. Therefore, at a relatively low reaction temperature like 250 °C, eventually the Cu{111} facet is blocked by COT and its derivatives because of the strong interaction between the Cu surface and the compound. It leads to two consequences, a terminated coupling reaction and stabilized Cu{111} facets. The reaction activity of the blocked facets dramatically drops, so that the coupling reaction is terminated. As a result, a concentration gradient of movable oligomers and the further derivatives between Cu{001}, Cu{110} facets and Cu{111} facets establishes since reaction products are accumulated unceasingly on Cu{001} and Cu{110} facets whereas the surface reaction terminates on Cu{111} facets. In the second step, the concentration gradient drives the movable oligomers and derivatives to diffuse from Cu{001} and Cu{110} facets to Cu{111} facets through the Cu surface, thus excess oligomers and derivatives precipitate on Cu{111} facets to build up CNs in the third step.

This model could be described as an adsorption (Vapor)—diffusion (Facet)—precipitation (Solid) process and then we name it as a VFS mechanism to distinguish from the classical VLS mechanism and vapor-solid-solid (VSS) mechanism [140], since a surface diffusion process of hydrocarbon dominates the whole process instead of bulk/surface diffusion of carbon atoms. This mechanism features: (i) Competition among different catalyst facets is the core factor (see Fig. 10). The facets on which C₂H₂ molecular is absorbed and coupled are defined as adsorbent facets, while the facets receiving coupling products and finally building up the CNs are defined as the growth facets. The adsorbent facets and the growth facets may reverse, depending on surface reactions and surface energies of the catalysts, which

Fig. 10 Sketch of the VFS growth mechanism: **a** C_2H_2 adsorbs on Cu surface, coupling to form different oligomers, movable ones on Cu{110} facets and immobilized ones on Cu {111} facets. **b** The immobilized oligomers block Cu{111} facets, and the movable oligomers diffuse from Cu{110} to Cu{111} facets. **c** Movable oligomers and further derivatives creep to overlay those immobilized oligomers and form nano-sheets during the diffusion [67]



are actually influenced by reaction temperatures and gaseous environment; (ii) The loose stacking nanostructure of polymer sheets allows the new build-up units to insert themselves into the gaps between existing nanofibers and the copper facets, and consequently to lift the old nanofibers up a bit to become a new part of the existing fiber. It presents that the existing nanofibers do not act a barrier blocking further the growth of themselves. (iii) Catalytic nanocrystals have undergone a surface reconstruction process, and turned into a regular appearance with certain low indexes and smooth facets, which correspond to its intrinsic symmetry.

4.4 The Applicability of VFS Mechanism

As the typical case of the low-temperature CVD growth of CNs, Cu catalyzed reaction is the most suitable one for the fundamental modeling research. Based on the model extracted from Cu/C₂H₂ reaction system, the growth with other transition metal catalysts can be interpreted. For example, in a growth which is based on Fe/C₂H₂ system and progressed at 350 °C, the Fe nanoparticle catalyst always exposes {110} face during growth. C₂H₂ is adsorbed on the active {110} face to form oligomers, and then the oligomers diffuse towards {001} face which is blocked by carbon and thus loses catalytic activity [64]. This process finally initiates the formation of CNs. Figure 11 shows related TEM images of the grown CNFs and schematically a possible growth route. Regardless of the detailed surface reactions and diffusion routes, the transportation and precipitation of aromatic species on the surface of the catalyst induce the growth of CNs. The surface processes can be generalized as a competition and cooperation between different catalytic crystalline faces. All these essential commons between the processes based on different catalysts illustrate an extensive adoptability of the proposed VFS mechanism for the explanation of low-temperature CVD growth of CNs on the metal catalyst.

With respect to the explanation of various morphologies of CNs, the VFS mechanism can be employed as well, since they only depend on the size and geometric features of the catalyst. For the highly symmetrical catalyst such as Cu nanocrystal, it causes symmetrically straight or helical nanofiber. It is also responsible for branched nanostructures when the Cu nanocrystal shows a more complex faceted shape. In cases that catalyst features a low symmetry, it results in a tip-grown nanofiber. The nanofiber can be solid or tubular. However, such a tubular product prepared at low temperatures is quite different from the CNT synthesized at high temperatures. The former has actually amorphous natures instead of graphitic walls.

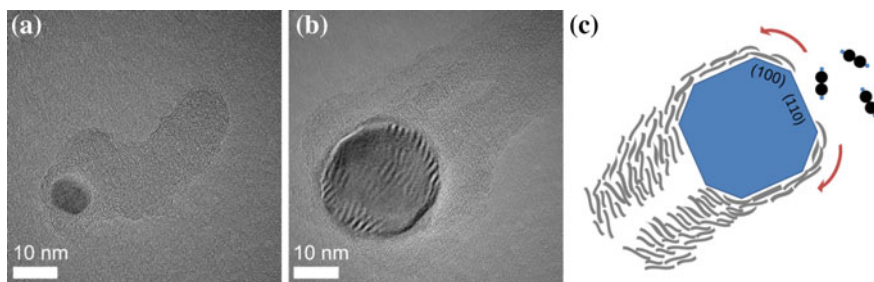


Fig. 11 TEM images of CNFs synthesized at 350 °C using Fe catalyst and C₂H₂ carbon source: **a** a solid nanofiber; **b** a tubular nanofiber; **c** sketch of the growth mechanism [64]

5 Enhanced Low-Temperature CVD Growth

Referred to the low-temperature CVD growth, it's necessary to mention a group of processes which are progressing with some enhancement factors, for example, plasma enhanced chemical vapor deposition (PECVD). By introducing plasma into the CVD growth, the process temperature was reduced remarkably [141–143], and then CNFs were even grown at room temperature [144]. However, the reported growth temperatures have been questioned due to the argument on temperature measurement [145]. In addition to the application of plasma, some other experimental setting also achieved enhancement effect on the CVD growth of CNs. For example, with the assistant of hot filament, CNFs were successfully synthesized at low temperatures [146–148]. The enhanced CVD growth concerns a lot of extra issues such as the complex plasma environment, the non-uniform heating, etc.

6 Applications

In terms of the one-dimensional carbon nanostructures synthesized via the low-temperature CVD method, their special morphologies, unusual atomic architectures as well as the properties associated with the unique growth mechanism grant them extensive applications. For example, Na et al. [61] synthesized densely packed CNT arrays on the conductive substrate at 400 °C. They were used in large-scale integrated circuits as interconnects to carry high density electric current [149]. The low process-temperature is compatible with other materials which are applied in semiconductor industry. Similar vertically aligned CNTs were also applied for field emission [58]. Qin et al. prepared pure carbon nanocoils (CNCs), and then coated these CNCs with Fe, Ni and Al_2O_3 with aid of atomic layer deposition (ALD) technique to synthesize $\text{Fe}_3\text{O}_4/\text{Al}_2\text{O}_3/\text{CNC}$ and $\text{Ni}/\text{Al}_2\text{O}_3/\text{CNC}$ coaxial multilayer nanostructures. The prepared magnetic CNCs showed enhanced microwave absorption properties [108]. This is attributed to the highly controllable morphologies of the synthesized CNCs. Furthermore since CNFs prepared via the low-temperature CVD method often feature disordered stacking graphene fragments, namely having large interlayer distances and abundant diffusion channels, these CNFs are therefore promising to be utilized as the anode of lithium-ion secondary batteries. They are supposed to bring high capacities and super-fast charge/discharge abilities. Meanwhile, they overcome the structural fragmentation during charge/discharge cycles. For example, no deterioration was found even after 85 cycles [91]. In addition, using such a low-temperature growth process in-situ doping of CNs is possible. The doped elements, such as nitrogen, silicon and boron will change the morphologies as well as the band structures of CNs. For instance, when the carbon anode in Li-ion secondary battery is doped by Si, the capacity was doubled, or even more. Doping nitrogen into CNTs not only improved the performance in supercapacitors [150, 151], but also resulted in a new application,

namely metal-free catalyst, which can be used in fuel cells to replace expensive Pt and Pd catalysts [152].

7 Summary

The growth of one dimensional carbon nanostructure is possible at relative low temperatures ($<450\text{ }^{\circ}\text{C}$). Nanoparticles from transition metal such as Fe, Co, Ni, their alloys, and Cu are the suitable catalysts for these low-temperature growths. The low-temperature thermal CVD process tends to produce amorphous carbon nanostructures rather than graphitic ones. Considerable hydrogen is often contained in the as-grown carbon nanostructures. Therefore these carbon nanostructures are polymer sheets. By means of tailoring the size and geometric features of the catalyst, precise morphology control of grown carbon nanostructure is achievable.

The classical VLS mechanism is not applicable to the low-temperature CVD process. An alternative model namely VFS mechanism has been proposed. It is based on the coupling of hydrocarbons (e.g., acetylene on metal surface) and subsequent surface diffusion of the coupling products. The core process in this mechanism is generalized as a competition and cooperation between different catalyst crystalline faces. This process results in the generation and transportation of carbon feedstock for the construction of carbon nanostructure. The rate-limiting step of the low-temperature CVD growth is the diffusion of carbon species through a pathway with a low activation energy on the surface of the catalyst, instead of the dissociation of carbon source gas. The fundamental structural unit, which diffuses on the surface of the catalyst and finally precipitates to construct carbon nanostructures, is most likely formed through catalytic reactions occurring on the surface of the metal catalyst.

The one-dimensional carbon nanostructures synthesized via the low-temperature CVD method have controllable special morphology, unusual atomic architecture as well as unique properties associated to the distinct VFS growth mechanism. These nanomaterials have the features of carbon materials as well as the unique properties of nanostructures. They are therefore promising as the absorbent for hazard materials in environmental clean-up, as the electrode for supercapacitors and lithium batteries, as well as the metal-free catalyst for different catalytic reactions.

Acknowledgements The authors would like to acknowledge financial support of this work by the German Research Foundation (DFG JI22/16-1, DFG JI22/21-1).

References

1. S. Iijima, Helical microtubules of graphitic carbon. *Nature* **354**(6348), 56–58 (1991). doi:[10.1038/354056a0](https://doi.org/10.1038/354056a0)
2. J. Hone, M.C. Llaguno, N.M. Nemes, A.T. Johnson, J.E. Fischer, D.A. Walters, M. J. Casavant, J. Schmidt, R.E. Smalley, Electrical and thermal transport properties of

- magnetically aligned single wall carbon nanotube films. *Appl. Phys. Lett.* **77**(5), 666–668 (2000). doi:[10.1063/1.127079](https://doi.org/10.1063/1.127079)
3. M.F. Yu, B.S. Files, S. Arepalli, R.S. Ruoff, Tensile loading of ropes of single wall carbon nanotubes and their mechanical properties. *Phys. Rev. Lett.* **84**(24), 5552–5555 (2000). doi:[10.1103/PhysRevLett.84.5552](https://doi.org/10.1103/PhysRevLett.84.5552)
 4. H. Kataura, Y. Kumazawa, Y. Maniwa, I. Umezu, S. Suzuki, Y. Ohtsuka, Y. Achiba, Optical properties of single-wall carbon nanotubes. *Synth. Met.* **103**(1–3), 2555–2558 (1999). doi:[10.1016/s0379-6779\(98\)00278-1](https://doi.org/10.1016/s0379-6779(98)00278-1)
 5. J.L. Hutchison, N.A. Kiselev, E.P. Krinichnaya, A.V. Krestinin, R.O. Loutfy, A.P. Morawsky, V.E. Muradyan, E.D. Obraztsova, J. Sloan, S.V. Terekhov, D.N. Zakharov, Double-walled carbon nanotubes fabricated by a hydrogen arc discharge method. *Carbon* **39**(5), 761–770 (2001). doi:[10.1016/s0008-6223\(00\)00187-1](https://doi.org/10.1016/s0008-6223(00)00187-1)
 6. E.G. Gamaly, T.W. Ebbesen, Mechanism of carbon nanotube formation in the arc-discharge. *Phys. Rev. B* **52**(3), 2083–2089 (1995). doi:[10.1103/PhysRevB.52.2083](https://doi.org/10.1103/PhysRevB.52.2083)
 7. C.D. Scott, S. Arepalli, P. Nikolaev, R.E. Smalley, Growth mechanisms for single-wall carbon nanotubes in a laser-ablation process. *Appl. Phys. A Mater. Sci. Process.* **72**(5), 573–580 (2001). doi:[10.1007/s003390100761](https://doi.org/10.1007/s003390100761)
 8. Y. Zhang, S. Iijima, Formation of single-wall carbon nanotubes by laser ablation of fullerenes at low temperature. *Appl. Phys. Lett.* **75**(20), 3087–3089 (1999). doi:[10.1063/1.125239](https://doi.org/10.1063/1.125239)
 9. A. Tanaka, S.H. Yoon, I. Mochida, Formation of fine Fe–Ni particles for the non-supported catalytic synthesis of uniform carbon nanofibers. *Carbon* **42**(7), 1291–1298 (2004). doi:[10.1016/j.carbon.2004.01.029](https://doi.org/10.1016/j.carbon.2004.01.029)
 10. J.H. Xia, X. Jiang, C.L. Jia, C. Dong, Hexahedral nanocementites catalyzing the growth of carbon nanohelices. *Appl. Phys. Lett.* **92**(6), 063121 (2008). doi:[10.1063/1.2842410](https://doi.org/10.1063/1.2842410)
 11. S. Motojima, Q.Q. Chen, Three-dimensional growth mechanism of cosmo-mimetic carbon microcoils obtained by chemical vapor deposition. *J. Appl. Phys.* **85**(7), 3919–3921 (1999). doi:[10.1063/1.369765](https://doi.org/10.1063/1.369765)
 12. G.Y. Zhang, X. Jiang, E.G. Wang, Tubular graphite cones. *Science* **300**(5618), 472–474 (2003). doi:[10.1126/science.1082264](https://doi.org/10.1126/science.1082264)
 13. X.S. Qi, W. Zhong, Y. Deng, C.T. Au, Y.W. Du, Characterization and magnetic properties of helical carbon nanotubes and carbon nanobelts synthesized in acetylene decomposition over Fe–Cu nanoparticles at 450 °C. *J. Phys. Chem. C* **113**(36), 15934–15940 (2009). doi:[10.1021/jp905387v](https://doi.org/10.1021/jp905387v)
 14. A.M. Cassell, J.A. Raymakers, J. Kong, H.J. Dai, Large scale CVD synthesis of single-walled carbon nanotubes. *J. Phys. Chem. B* **103**(31), 6484–6492 (1999). doi:[10.1021/jp990957s](https://doi.org/10.1021/jp990957s)
 15. E. Couteau, K. Hernadi, J.W. Seo, L. Thien-Nga, C. Miko, R. Gaal, L. Forro, CVD synthesis of high-purity multiwalled carbon nanotubes using CaCO₃ catalyst support for large-scale production. *Chem. Phys. Lett.* **378**(1–2), 9–17 (2003). doi:[10.1016/s0009-2614\(03\)01218-1](https://doi.org/10.1016/s0009-2614(03)01218-1)
 16. Y.A. Kim, T. Hayashi, S. Naokawa, T. Yanaisawa, M. Endo, Comparative study of herringbone and stacked-cup carbon nanofibers. *Carbon* **43**(14), 3005–3008 (2005). doi:[10.1016/j.carbon.2005.06.037](https://doi.org/10.1016/j.carbon.2005.06.037)
 17. Y.A. Zhu, Z.J. Sui, T.J. Zhao, Y.C. Dai, Z.M. Cheng, W.K. Yuan, Modeling of fishbone-type carbon nanofibers: a theoretical study. *Carbon* **43**(8), 1694–1699 (2005). doi:[10.1016/j.carbon.2005.02.011](https://doi.org/10.1016/j.carbon.2005.02.011)
 18. A. de Lucas, P.B. Garcia, A. Garrido, A. Romero, J.L. Valverde, Catalytic synthesis of carbon nanofibers with different graphene plane alignments using Ni deposited on iron pillared clays. *Appl. Catal. A Gen.* **301**(1), 123–132 (2006). doi:[10.1016/j.apcata.2005.11.026](https://doi.org/10.1016/j.apcata.2005.11.026)
 19. H. Cui, O. Zhou, B.R. Stoner, Deposition of aligned bamboo-like carbon nanotubes via microwave plasma enhanced chemical vapor deposition. *J. Appl. Phys.* **88**(10), 6072–6074 (2000). doi:[10.1063/1.1320024](https://doi.org/10.1063/1.1320024)
 20. C.J. Lee, J. Park, Growth model of bamboo-shaped carbon nanotubes by thermal chemical vapor deposition. *Appl. Phys. Lett.* **77**(21), 3397–3399 (2000). doi:[10.1063/1.1320851](https://doi.org/10.1063/1.1320851)

21. C.J. Lee, J.H. Park, J. Park, Synthesis of bamboo-shaped multiwalled carbon nanotubes using thermal chemical vapor deposition. *Chem. Phys. Lett.* **323**(5–6), 560–565 (2000). doi:[10.1016/s0009-2614\(00\)00548-0](https://doi.org/10.1016/s0009-2614(00)00548-0)
22. M. Lin, J.P.Y. Tan, C. Boothroyd, K.P. Loh, E.S. Tok, Y.L. Foo, Dynamical observation of bamboo-like carbon nanotube growth. *Nano Lett.* **7**(8), 2234–2238 (2007). doi:[10.1021/nl070681x](https://doi.org/10.1021/nl070681x)
23. J.P. Tu, L.P. Zhu, K. Hou, S.Y. Guo, Synthesis and frictional properties of array film of amorphous carbon nanofibers on anodic aluminum oxide. *Carbon* **41**(6), 1257–1263 (2003). doi:[10.1016/s0008-6223\(03\)00047-2](https://doi.org/10.1016/s0008-6223(03)00047-2)
24. Z.W. Pan, S.S. Xie, B.H. Chang, L.F. Sun, W.Y. Zhou, G. Wang, Direct growth of aligned open carbon nanotubes by chemical vapor deposition. *Chem. Phys. Lett.* **299**(1), 97–102 (1999). doi:[10.1016/s0009-2614\(98\)01240-8](https://doi.org/10.1016/s0009-2614(98)01240-8)
25. M.J. de Andrade, M.D. Lima, C.P. Bergmann, G.D. Ramminger, N.M. Balzaretto, T.M.H. Costa, M.R. Gallas, Carbon nanotube/silica composites obtained by sol-gel and high-pressure techniques. *Nanotechnology* **19**(26), 265607 (2008). doi:[10.1088/0957-4484/19/26/265607](https://doi.org/10.1088/0957-4484/19/26/265607)
26. R.R. Bacsa, C. Laurent, A. Peigney, W.S. Bacsa, T. Vaugien, A. Rousset, High specific surface area carbon nanotubes from catalytic chemical vapor deposition process. *Chem. Phys. Lett.* **323**(5–6), 566–571 (2000). doi:[10.1016/s0009-2614\(00\)00558-3](https://doi.org/10.1016/s0009-2614(00)00558-3)
27. J.P. Pinheiro, M.C. Schouler, P. Gadelle, Nanotubes and nanofilaments from carbon monoxide disproportionation over Co/MgO catalysts I. Growth versus catalyst state. *Carbon* **41**(15), 2949–2959 (2003). doi:[10.1016/s0008-6223\(03\)00410-x](https://doi.org/10.1016/s0008-6223(03)00410-x)
28. Y.M. Li, W. Kim, Y.G. Zhang, M. Rolandi, D.W. Wang, H.J. Dai, Growth of single-walled carbon nanotubes from discrete catalytic nanoparticles of various sizes. *J. Phys. Chem. B* **105**(46), 11424–11431 (2001). doi:[10.1021/jp012085b](https://doi.org/10.1021/jp012085b)
29. D. Venegoni, P. Serp, R. Feurer, Y. Kihn, C. Vahlas, P. Kalck, Parametric study for the growth of carbon nanotubes by catalytic chemical vapor deposition in a fluidized bed reactor. *Carbon* **40**(10), 1799–1807 (2002). doi:[10.1016/s0008-6223\(02\)00057-x](https://doi.org/10.1016/s0008-6223(02)00057-x)
30. K. Hernadi, A. Fonseca, J.B. Nagy, D. Bernaerts, A. Fudala, A.A. Lucas, Catalytic synthesis of carbon nanotubes using zeolite support. *Zeolites* **17**(5–6), 416–423 (1996). doi:[10.1016/s0144-2449\(96\)00088-7](https://doi.org/10.1016/s0144-2449(96)00088-7)
31. H. Ago, T. Komatsu, S. Ohshima, Y. Kuriki, M. Yumura, Dispersion of metal nanoparticles for aligned carbon nanotube arrays. *Appl. Phys. Lett.* **77**(1), 79–81 (2000). doi:[10.1063/1.126883](https://doi.org/10.1063/1.126883)
32. Y. Li, J. Liu, Y.Q. Wang, Z.L. Wang, Preparation of monodispersed Fe–Mo nanoparticles as the catalyst for CVD synthesis of carbon nanotubes. *Chem. Mater.* **13**(3), 1008–1014 (2001). doi:[10.1021/cm000787s](https://doi.org/10.1021/cm000787s)
33. C.L. Cheung, A. Kurtz, H. Park, C.M. Lieber, Diameter-controlled synthesis of carbon nanotubes. *J. Phys. Chem. B* **106**(10), 2429–2433 (2002). doi:[10.1021/jp0142278](https://doi.org/10.1021/jp0142278)
34. Y. Qin, Z.K. Zhang, Z.L. Cui, Helical carbon nanofibers with a symmetric growth mode. *Carbon* **42**(10), 1917–1922 (2004). doi:[10.1016/j.carbon.2004.03.020](https://doi.org/10.1016/j.carbon.2004.03.020)
35. N.G. Shang, X. Jiang, Large-sized tubular graphite cones with nanotube tips. *Appl. Phys. Lett.* **87**(16), 163102 (2005). doi:[10.1063/1.2093919](https://doi.org/10.1063/1.2093919)
36. N.G. Shang, W.I. Milne, X. Jiang, Tubular graphite cones with single-crystal nanotips and their antioxygenic properties. *J. Am. Chem. Soc.* **129**(28), 8907–8911 (2007). doi:[10.1021/ja071830g](https://doi.org/10.1021/ja071830g)
37. G.Y. Zhang, X.C. Ma, D.Y. Zhong, E.G. Wang, Polymerized carbon nitride nanobells. *J. Appl. Phys.* **91**(11), 9324–9332 (2002). doi:[10.1063/1.1476070](https://doi.org/10.1063/1.1476070)
38. Y.G. Zhang, A.L. Chang, J. Cao, Q. Wang, W. Kim, Y.M. Li, N. Morris, E. Yenilmez, J. Kong, H.J. Dai, Electric-field-directed growth of aligned single-walled carbon nanotubes. *Appl. Phys. Lett.* **79**(19), 3155–3157 (2001). doi:[10.1063/1.1415412](https://doi.org/10.1063/1.1415412)
39. A. Ural, Y.M. Li, H.J. Dai, Electric-field-aligned growth of single-walled carbon nanotubes on surfaces. *Appl. Phys. Lett.* **81**(18), 3464–3466 (2002). doi:[10.1063/1.1518773](https://doi.org/10.1063/1.1518773)

40. R.S. Wagner, W.C. Ellis, Vapor-liquid-solid mechanism of single crystal growth (New method growth catalysis from impurity whisker epitaxial + large crystals Si E). *Appl. Phys. Lett.* **4**(5), 89 (1964). doi:[10.1063/1.1753975](https://doi.org/10.1063/1.1753975)
41. H. Kanzow, A. Ding, Formation mechanism of single-wall carbon nanotubes on liquid-metal particles. *Phys. Rev. B* **60**(15), 11180–11186 (1999). doi:[10.1103/PhysRevB.60.11180](https://doi.org/10.1103/PhysRevB.60.11180)
42. M.A. Ermakova, D.Y. Ermakov, A.L. Chuvilin, G.G. Kuvshinov, Decomposition of methane over iron catalysts at the range of moderate temperatures: the influence of structure of the catalytic systems and the reaction conditions on the yield of carbon and morphology of carbon filaments. *J. Catal.* **201**(2), 183–197 (2001). doi:[10.1006/jcat.2001.3243](https://doi.org/10.1006/jcat.2001.3243)
43. Y. Shibuta, S. Maruyama, Molecular dynamics simulation of formation process of single-walled carbon nanotubes by CCVD method. *Chem. Phys. Lett.* **382**(3–4), 381–386 (2003). doi:[10.1016/j.cplett.2003.10.080](https://doi.org/10.1016/j.cplett.2003.10.080)
44. S. Tsunekawa, S. Ito, Y. Kawazoe, J.T. Wang, Critical size of the phase transition from cubic to tetragonal in pure zirconia nanoparticles. *Nano Lett.* **3**(7), 871–875 (2003). doi:[10.1021/nl034129t](https://doi.org/10.1021/nl034129t)
45. S.S. Fan, W.J. Liang, H.Y. Dang, N. Franklin, T. Tomblor, M. Chapline, H.J. Dai, Carbon nanotube arrays on silicon substrates and their possible application. *Physica E* **8**(2), 179–183 (2000). doi:[10.1016/s1386-9477\(00\)00136-3](https://doi.org/10.1016/s1386-9477(00)00136-3)
46. R.T.K. Baker, Catalytic growth of carbon filaments. *Carbon* **27**(3), 315–323 (1989). doi:[10.1016/0008-6223\(89\)90062-6](https://doi.org/10.1016/0008-6223(89)90062-6)
47. J. Gavillet, A. Loiseau, C. Journet, F. Willaime, F. Ducastelle, J.C. Charlier, Root-growth mechanism for single-wall carbon nanotubes. *Phys. Rev. Lett.* **87**(27), 275504 (2001). doi:[10.1103/PhysRevLett.87.275504](https://doi.org/10.1103/PhysRevLett.87.275504)
48. N.M. Rodriguez, A. Chambers, R.T.K. Baker, Catalytic engineering of carbon nanostructures. *Langmuir* **11**(10), 3862–3866 (1995). doi:[10.1021/la00010a042](https://doi.org/10.1021/la00010a042)
49. R.T. Yang, J.P. Chen, Mechanism of carbon-filament growth on metal-catalysts. *J. Catal.* **115**(1), 52–64 (1989). doi:[10.1016/0021-9517\(89\)90006-7](https://doi.org/10.1016/0021-9517(89)90006-7)
50. J.A. Lobo, G.H. Geiger, Thermodynamics and solubility of carbon in ferrite and ferritic Fe–Mo alloys. *Metall. Trans. A Phys. Metall. Mater. Sci.* **7**(9), 1347–1357 (1976). doi:[10.1007/bf02658820](https://doi.org/10.1007/bf02658820)
51. C.P. Deck, K. Vecchio, Prediction of carbon nanotube growth success by the analysis of carbon-catalyst binary phase diagrams. *Carbon* **44**(2), 267–275 (2006). doi:[10.1016/j.carbon.2005.07.023](https://doi.org/10.1016/j.carbon.2005.07.023)
52. T. Maruyama, K. Sato, Y. Mizutani, K. Tanioku, T. Shiraiwa, S. Naritsuka, Low-temperature synthesis of single-walled carbon nanotubes by alcohol gas source growth in high vacuum. *J. Nanosci. Nanotechnol.* **10**(6), 4095–4101 (2010). doi:[10.1166/jnn.2010.2000](https://doi.org/10.1166/jnn.2010.2000)
53. J. Highfield, Y.S. Loo, Z. Zhong, B. Grushko, Thermogravimetric studies of carbon nanofiber formation from methane at low temperature over Ni-based skeletal catalysts and the effect of substrate pre-carburization. *Carbon* **45**(13), 2597–2607 (2007). doi:[10.1016/j.carbon.2007.08.012](https://doi.org/10.1016/j.carbon.2007.08.012)
54. D. He, J. Bai, Acetylene-enhanced growth of carbon nanotubes on ceramic microparticles for multi-scale hybrid structures. *Chem. Vap. Depos.* **17**(4–6), 98–106 (2011). doi:[10.1002/cvde.201006878](https://doi.org/10.1002/cvde.201006878)
55. A. Magrez, J.W. Seo, R. Smajda, B. Korbely, J.C. Andresen, M. Mionic, S. Casimirius, L. Forro, Low-temperature, highly efficient growth of carbon nanotubes on functional materials by an oxidative dehydrogenation reaction. *ACS Nano* **4**(7), 3702–3708 (2010). doi:[10.1021/nn100279j](https://doi.org/10.1021/nn100279j)
56. N. Halonen, A. Sapi, L. Nagy, R. Puskas, A.-R. Leino, J. Maklin, J. Kukkola, G. Toth, M.-C. Wu, H.-C. Liao, W.-F. Su, A. Shchukarev, J.-P. Mikkola, A. Kukovecz, Z. Konya, K. Kordas, Low-temperature growth of multi-walled carbon nanotubes by thermal CVD. *Physica Status Solidi B Basic Solid State Phys.* **248**(11), 2500–2503 (2011). doi:[10.1002/pspb.201100137](https://doi.org/10.1002/pspb.201100137)
57. O. Pitkanen, N. Halonen, A.R. Leino, J. Maklin, A. Dombovari, J.H. Lin, G. Toth, K. Kordas, Low-temperature growth of carbon nanotubes on bi- and tri-metallic catalyst templates. *Top. Catal.* **56**(9–10), 522–526 (2013). doi:[10.1007/s11244-013-0047-9](https://doi.org/10.1007/s11244-013-0047-9)

58. Y.M. Shyu, F.C.N. Hong, Low-temperature growth and field emission of aligned carbon nanotubes by chemical vapor deposition. *Mater. Chem. Phys.* **72**(2), 223–227 (2001). doi:[10.1016/s0254-0584\(01\)00441-2](https://doi.org/10.1016/s0254-0584(01)00441-2)
59. Y.M. Shyu, F.C.N. Hong, The effects of pre-treatment and catalyst composition on growth of carbon nanofibers at low temperature. *Diam. Relat. Mater.* **10**(3–7), 1241–1245 (2001). doi:[10.1016/s0925-9635\(00\)00550-1](https://doi.org/10.1016/s0925-9635(00)00550-1)
60. K. Aoki, T. Yamamoto, H. Furuta, T. Ikuno, S. Honda, M. Furuta, K. Oura, T. Hirao, Low-temperature growth of carbon nanofiber by thermal chemical vapor deposition using CuNi catalyst. *Jpn. J. Appl. Phys. Part 1 Regular Pap. Brief Commun. Rev. Pap.* **45**(6A), 5329–5331 (2006). doi:[10.1143/jjap.45.5329](https://doi.org/10.1143/jjap.45.5329)
61. N. Na, D.Y. Kim, Y.-G. So, Y. Ikuhara, S. Noda, Simple and engineered process yielding carbon nanotube arrays with $1.2 \times 10^{13} \text{ cm}^{-2}$ wall density on conductive underlayer at 400 °C. *Carbon* **81**, 773–781 (2015). doi:[10.1016/j.carbon.2014.10.023](https://doi.org/10.1016/j.carbon.2014.10.023)
62. K. Tanioku, T. Maruyama, S. Naritsuka, Low temperature growth of carbon nanotubes on Si substrates in high vacuum. *Diam. Relat. Mater.* **17**(4–5), 589–593 (2008). doi:[10.1016/j.diamond.2007.10.028](https://doi.org/10.1016/j.diamond.2007.10.028)
63. X. Li, Z. Xu, One-step catalytic growth of carbon nanofiber arrays vertically aligned on carbon substrate. *Mater. Res. Bull.* **47**(6), 1557–1561 (2012). doi:[10.1016/j.materresbull.2012.02.027](https://doi.org/10.1016/j.materresbull.2012.02.027)
64. Y. Ma, C. Weimer, N. Yang, L. Zhang, T. Staedler, X. Jiang, Low-temperature growth of carbon nanofiber using a vapor–facet–solid process. *Mater. Today Commun.* **2**, e55–e61 (2015). doi:[10.1016/j.mtcomm.2014.12.003](https://doi.org/10.1016/j.mtcomm.2014.12.003)
65. B. Yu, S. Wang, Q. Zhang, Y. He, H. Huang, J. Zou, Ni₃C-assisted growth of carbon nanofibres 300 °C by thermal CVD. *Nanotechnology* **25**(32), 325602 (2014). doi:[10.1088/0957-4484/25/32/325602](https://doi.org/10.1088/0957-4484/25/32/325602)
66. W.-H. Chiang, R.M. Sankaran, Synergistic effects in bimetallic nanoparticles for low temperature carbon nanotube growth. *Adv. Mater.* **20**(24), 4857–4861 (2008). doi:[10.1002/adma.200801006](https://doi.org/10.1002/adma.200801006)
67. Y. Ma, X. Sun, N. Yang, J. Xia, L. Zhang, X. Jiang, Shape-controlled growth of carbon nanostructures: yield and mechanism. *Chem. Eur. J.* **21**, 12370–12375 (2015). doi:[10.1002/chem.201500440](https://doi.org/10.1002/chem.201500440)
68. Y. Qin, Q. Zhang, Z.L. Cui, Effect of synthesis method of nanocopper catalysts on the morphologies of carbon nanofibers prepared by catalytic decomposition of acetylene. *J. Catal.* **223**(2), 389–394 (2004). doi:[10.1016/j.jcat.2004.02.004](https://doi.org/10.1016/j.jcat.2004.02.004)
69. J.H. Xia, X. Jiang, C.L. Jia, The size effect of catalyst on the growth of helical carbon nanofibers. *Appl. Phys. Lett.* **95**(22), 223110 (2009). doi:[10.1063/1.3271031](https://doi.org/10.1063/1.3271031)
70. Y. Qin, M. Eggers, T. Staedler, X. Jiang, Symmetric growth of carbon nanosheets on Cu nanowires by a surface diffusion mechanism. *Nanotechnology* **18**(34), 345607 (2007). doi:[10.1088/0957-4484/18/34/345607](https://doi.org/10.1088/0957-4484/18/34/345607)
71. Y. Qin, X. Jiang, Z.L. Cui, Low-temperature synthesis of amorphous carbon nanocoils via acetylene coupling on copper nanocrystal surfaces at 468 K: a reaction mechanism analysis. *J. Phys. Chem. B* **109**(46), 21749–21754 (2005). doi:[10.1021/jp054412b](https://doi.org/10.1021/jp054412b)
72. X. Sun, Y.W. Zhang, R. Si, C.H. Yan, Metal (mn Co, and Cu) oxide nanocrystals from simple formate precursors. *Small* **1**(11), 1081–1086 (2005). doi:[10.1002/sml.200500119](https://doi.org/10.1002/sml.200500119)
73. J.H. Xia, Growth of carbon nanofibers studied by using transmission electron microscopy. Shaker Verlag, D-52018 Aachen (2010)
74. A.J. Hart, A.H. Slocum, L. Royer, Growth of conformal single-walled carbon nanotube films from Mo/Fe/Al₂O₃ deposited by electron beam evaporation. *Carbon* **44**(2), 348–359 (2006). doi:[10.1016/j.carbon.2005.07.008](https://doi.org/10.1016/j.carbon.2005.07.008)
75. Y.J. Tian, Z. Hu, Y. Yang, X.Z. Wang, X. Chen, H. Xu, Q. Wu, W.J. Ji, Y. Chen, In situ TA-MS study of the six-membered-ring-based growth of carbon nanotubes with benzene precursor. *J. Am. Chem. Soc.* **126**(4), 1180–1183 (2004). doi:[10.1021/ja037561i](https://doi.org/10.1021/ja037561i)

76. B. Zheng, C.G. Lu, G. Gu, A. Makarovski, G. Finkelstein, J. Liu, Efficient CVD growth of single-walled carbon nanotubes on surfaces using carbon monoxide precursor. *Nano Lett.* **2**(8), 895–898 (2002). doi:[10.1021/nl025634d](https://doi.org/10.1021/nl025634d)
77. A.J. Hart, A.H. Slocum, Rapid growth and flow-mediated nucleation of millimeter-scale aligned carbon nanotube structures from a thin-film catalyst. *J. Phys. Chem. B.* **110**(16), 8250–8257 (2006). doi:[10.1021/jp055498b](https://doi.org/10.1021/jp055498b)
78. M. Jung, K.Y. Eun, J.K. Lee, Y.J. Baik, K.R. Lee, J.W. Park, Growth of carbon nanotubes by chemical vapor deposition. *Diam. Relat. Mater.* **10**(3–7), 1235–1240 (2001). doi:[10.1016/s0925-9635\(00\)00446-5](https://doi.org/10.1016/s0925-9635(00)00446-5)
79. A.V. Vasenkov, D. Sengupta, M. Frenklach, Multiscale modeling catalytic decomposition of hydrocarbons during carbon nanotube growth. *J. Phys. Chem. B.* **113**(7), 1877–1882 (2009). doi:[10.1021/jp808346h](https://doi.org/10.1021/jp808346h)
80. G.D. Nessim, A. Al-Obeidi, H. Grisaru, E.S. Polsen, C.R. Oliver, T. Zimrin, A.J. Hart, D. Aurbach, C.V. Thompson, Synthesis of tall carpets of vertically aligned carbon nanotubes by in situ generation of water vapor through preheating of added oxygen. *Carbon* **50**(11), 4002–4009 (2012). doi:[10.1016/j.carbon.2012.04.043](https://doi.org/10.1016/j.carbon.2012.04.043)
81. D.N. Futaba, K. Hata, T. Yamada, K. Mizuno, M. Yumura, S. Iijima, Kinetics of water-assisted single-walled carbon nanotube synthesis revealed by a time-evolution analysis. *Phys. Rev. Lett.* **95**(5), 4 (2005). doi:[10.1103/PhysRevLett.95.056104](https://doi.org/10.1103/PhysRevLett.95.056104)
82. S. Hussain, R. Amade, E. Bertran, Study of CNTs structural evolution during water assisted growth and transfer methodology for electrochemical applications. *Mater. Chem. Phys.* **148**(3), 914–922 (2014). doi:[10.1016/j.matchemphys.2014.08.070](https://doi.org/10.1016/j.matchemphys.2014.08.070)
83. M. Bansal, C. Lal, R. Srivastava, M.N. Kamalasanan, L.S. Tanwar, Comparison of structure and yield of multiwall carbon nanotubes produced by the CVD technique and a water assisted method. *Physica B Condens. Matter* **405**(7), 1745–1749 (2010). doi:[10.1016/j.physb.2010.01.031](https://doi.org/10.1016/j.physb.2010.01.031)
84. C.-S. Chen, C.-K. Hsieh, Oxygen-assisted low-pressure chemical vapor deposition for the low-temperature direct growth of graphitic nanofibers on fluorine-doped tin oxide glass as a counter electrode for dye-sensitized solar cell. *Jpn. J. Appl. Phys.* **53**(11), 11RE02 (2014). doi:[10.7567/jjap.53.11re02](https://doi.org/10.7567/jjap.53.11re02)
85. I.H. Son, H.J. Song, S. Kwon, A. Bachmatiuk, S.J. Lee, A. Benayad, J.H. Park, J.-Y. Choi, H. Chang, M.H. Ruemmeli, CO₂ enhanced chemical vapor deposition growth of few-layer graphene over NiO_x. *ACS Nano* **8**(9), 9224–9232 (2014). doi:[10.1021/nn504342e](https://doi.org/10.1021/nn504342e)
86. J.Q. Huang, Q. Zhang, M.Q. Zhao, F. Wei, Process intensification by CO₂ for high quality carbon nanotube forest growth: double-walled carbon nanotube convexity or single-walled carbon nanotube bowls? *Nano Res.* **2**(11), 872–881 (2009). doi:[10.1007/s12274-009-9088-6](https://doi.org/10.1007/s12274-009-9088-6)
87. Z. Zhu, H. Jiang, T. Susi, A.G. Nasibulin, E.I. Kauppinen, The use of NH₃ to promote the production of large-diameter single-walled carbon nanotubes with a narrow (n, m) distribution. *J. Am. Chem. Soc.* **133**(5), 1224–1227 (2011). doi:[10.1021/ja1087634](https://doi.org/10.1021/ja1087634)
88. T. Susi, A.G. Nasibulin, P. Ayala, Y. Tian, Z. Zhu, H. Jiang, C. Roquelet, D. Garrot, J.-S. Lauret, E.I. Kauppinen, High quality SWCNT synthesis in the presence of NH₃ using a vertical flow aerosol reactor. *Physica Status Solidi B Basic Solid State Phys.* **246**(11–12), 2507–2510 (2009). doi:[10.1002/pssb.200982338](https://doi.org/10.1002/pssb.200982338)
89. A.F. Carley, P.R. Davies, K.R. Harikumar, R.V. Jones, M.W. Roberts, Oxygen states at magnesium and copper surfaces revealed by scanning tunneling microscopy and surface reactivity. *Top. Catal.* **24**(1–4), 51–59 (2003). doi:[10.1023/B:TOCA.0000003076.82649.c4](https://doi.org/10.1023/B:TOCA.0000003076.82649.c4)
90. P.R. Davies, D. Edwards, D. Richards, Possible role for Cu(II) compounds in the oxidation of malonyl dichloride and HCl at Cu (110) surfaces. *J. Phys. Chem. C* **113**(24), 10333–10336 (2009). doi:[10.1021/jp903042f](https://doi.org/10.1021/jp903042f)
91. Y. Ma, Vapor-facet-solid (VFS) mechanism: a new route for catalytic CVD growth of one-dimensional nanostructures at low temperature. *Schriftenreihe der Arbeitsgruppe des Lehrstuhls für Oberflächen- und Werkstofftechnologie im Institut für Werkstofftechnik.* **4** (2015)

92. J.T. Hu, L.S. Li, W.D. Yang, L. Manna, L.W. Wang, A.P. Alivisatos, Linearly polarized emission from colloidal semiconductor quantum rods. *Science* **292**(5524), 2060–2063 (2001). doi:[10.1126/science.1060810](https://doi.org/10.1126/science.1060810)
93. A.X. Yin, X.Q. Min, Y.W. Zhang, C.H. Yan, Shape-selective synthesis and facet-dependent enhanced electrocatalytic activity and durability of monodisperse sub-10 nm Pt-Pd tetrahedrons and cubes. *J. Am. Chem. Soc.* **133**(11), 3816–3819 (2011). doi:[10.1021/ja200329p](https://doi.org/10.1021/ja200329p)
94. S. Mostafa, F. Behafarid, J.R. Croy, L.K. Ono, L. Li, J.C. Yang, A.I. Frenkel, B.R. Cuenya, Shape-dependent catalytic properties of Pt nanoparticles. *J. Am. Chem. Soc.* **132**(44), 15714–15719 (2010). doi:[10.1021/ja106679z](https://doi.org/10.1021/ja106679z)
95. H. Zhang, M.S. Jin, Y.J. Xiong, B. Lim, Y.N. Xia, Shape-controlled synthesis of Pd nanocrystals and their catalytic applications. *Acc. Chem. Res.* **46**(8), 1783–1794 (2013). doi:[10.1021/ar300209w](https://doi.org/10.1021/ar300209w)
96. R. Narayanan, M.A. El-Sayed, Catalysis with transition metal nanoparticles in colloidal solution: nanoparticle shape dependence and stability. *J. Phys. Chem. B.* **109**(26), 12663–12676 (2005). doi:[10.1021/jp051066p](https://doi.org/10.1021/jp051066p)
97. Y.H. Leng, Y.H. Zhang, T. Liu, M. Suzuki, X.G. Li, Synthesis of single crystalline triangular and hexagonal Ni nanosheets with enhanced magnetic properties. *Nanotechnology* **17**(6), 1797–1800 (2006). doi:[10.1088/0957-4484/17/6/042](https://doi.org/10.1088/0957-4484/17/6/042)
98. Y.W. Jun, J.S. Choi, J. Cheon, Shape control of semiconductor and metal oxide nanocrystals through nonhydrolytic colloidal routes. *Angewandte Chemie International Edition* **45**(21), 3414–3439 (2006). doi:[10.1002/anie.200503821](https://doi.org/10.1002/anie.200503821)
99. Y.N. Xia, Y.J. Xiong, B. Lim, S.E. Skrabalak, Shape-controlled synthesis of metal nanocrystals: simple chemistry meets complex physics? *Angewandte Chemie International Edition* **48**(1), 60–103 (2009). doi:[10.1002/anie.200802248](https://doi.org/10.1002/anie.200802248)
100. A.R. Tao, S. Habas, P.D. Yang, Shape control of colloidal metal nanocrystals. *Small* **4**(3), 310–325 (2008). doi:[10.1002/smll.200701295](https://doi.org/10.1002/smll.200701295)
101. E.F. Kukovitsky, S.G. L'Vov, N.A. Sainov, VLS-growth of carbon nanotubes from the vapor. *Chem. Phys. Lett.* **317**(1–2), 65–70 (2000). doi:[10.1016/s0009-2614\(99\)01299-3](https://doi.org/10.1016/s0009-2614(99)01299-3)
102. B.C. Satishkumar, P.J. Thomas, A. Govindaraj, C.N.R. Rao, Y-junction carbon nanotubes. *Appl. Phys. Lett.* **77**(16), 2530–2532 (2000). doi:[10.1063/1.1319185](https://doi.org/10.1063/1.1319185)
103. J. Li, C. Papadopoulos, J. Xu, Nanoelectronics—growing Y-junction carbon nanotubes. *Nature* **402**(6759), 253–254 (1999). doi:[10.1038/46214](https://doi.org/10.1038/46214)
104. H. Takikawa, M. Yatsuki, R. Miyano, M. Nagayama, T. Sakakibara, S. Itoh, Y. Ando, Amorphous carbon fibrilliform nanomaterials prepared by chemical vapor deposition. *Jpn. J. Appl. Phys. Part 1 Regular Pap. Short Notes Rev. Pap.* **39**(9A), 5177–5179 (2000). doi:[10.1143/jjap.39.5177](https://doi.org/10.1143/jjap.39.5177)
105. K. Inomata, N. Aoki, H. Koinuma, Production of fullerenes by low-temperature plasma chemical-vapor-deposition under atmospheric-pressure. *Jpn. J. Appl. Phys. Part 2 Lett.* **33**(2A), L197–L199 (1994). doi:[10.1143/jjap.33.1197](https://doi.org/10.1143/jjap.33.1197)
106. Y. Suda, Y. Shimizu, M. Ozaki, H. Tanoue, H. Takikawa, H. Ue, K. Shimizu, Y. Umeda, Electrochemical properties of fuel cell catalysts loaded on carbon nanomaterials with different geometries. *Mater. Today Commun.* **3**, 96–103 (2015). doi:[10.1016/j.mtcomm.2015.02.003](https://doi.org/10.1016/j.mtcomm.2015.02.003)
107. G. Wang, G. Ran, G. Wan, P. Yang, Z. Gao, S. Lin, C. Fu, Y. Qin, Size-selective catalytic growth of nearly 100 % pure carbon nanocoils with copper nanoparticles produced by atomic layer deposition. *ACS Nano* **8**(5), 5330–5338 (2014). doi:[10.1021/mn501709h](https://doi.org/10.1021/mn501709h)
108. G. Wang, Z. Gao, S. Tang, C. Chen, F. Duan, S. Zhao, S. Lin, Y. Feng, L. Zhou, Y. Qin, Microwave absorption properties of carbon nanocoils coated with highly controlled magnetic materials by atomic layer deposition. *ACS Nano* **6**(12), 11009–11017 (2012). doi:[10.1021/mn304630h](https://doi.org/10.1021/mn304630h)

109. K. Hernadi, A. Fonseca, J.B. Nagy, D. Bernaerts, A.A. Lucas, Fe-catalyzed carbon nanotube formation. *Carbon* **34**(10), 1249–1257 (1996). doi:[10.1016/0008-6223\(96\)00074-7](https://doi.org/10.1016/0008-6223(96)00074-7)
110. D. Chen, K.O. Christensen, E. Ochoa-Fernandez, Z.X. Yu, B. Totdal, N. Latorre, A. Monzon, A. Holmen, Synthesis of carbon nanofibers: effects of Ni crystal size during methane decomposition. *J. Catal.* **229**(1), 82–96 (2005). doi:[10.1016/j.jcat.2004.10.017](https://doi.org/10.1016/j.jcat.2004.10.017)
111. P.L. Hansen, J.B. Wagner, S. Helveg, J.R. Rostrup-Nielsen, B.S. Clausen, H. Topsøe, Atom-resolved imaging of dynamic shape changes in supported copper nanocrystals. *Science* **295**(5562), 2053–2055 (2002). doi:[10.1126/science.1069325](https://doi.org/10.1126/science.1069325)
112. C.A. Wert, Diffusion coefficient of C in α -iron. *Phys. Rev.* **79**(4), 601–605 (1950). doi:[10.1103/PhysRev.79.601](https://doi.org/10.1103/PhysRev.79.601)
113. J.J. Lander, H.E. Kern, A.L. Beach, Solubility and diffusion coefficient of carbon in nickel—reaction rates of nickel–carbon alloys with barium oxide. *J. Appl. Phys.* **23**(12), 1305–1309 (1952). doi:[10.1063/1.1702064](https://doi.org/10.1063/1.1702064)
114. B.C. Stipe, M.A. Rezaei, W. Ho, Single-molecule vibrational spectroscopy and microscopy. *Science* **280**(5370), 1732–1735 (1998). doi:[10.1126/science.280.5370.1732](https://doi.org/10.1126/science.280.5370.1732)
115. B.C. Stipe, M.A. Rezaei, W. Ho, Coupling of vibrational excitation to the rotational motion of a single adsorbed molecule. *Phys. Rev. Lett.* **81**(6), 1263–1266 (1998). doi:[10.1103/PhysRevLett.81.1263](https://doi.org/10.1103/PhysRevLett.81.1263)
116. J. Szanyi, M.T. Paffett, Dimerization and trimerization of acetylene over a model Sn/Pt catalyst. *J. Am. Chem. Soc.* **117**(3), 1034–1042 (1995). doi:[10.1021/ja00108a020](https://doi.org/10.1021/ja00108a020)
117. S. Helveg, C. Lopez-Cartes, J. Sehested, P.L. Hansen, B.S. Clausen, J.R. Rostrup-Nielsen, F. Abild-Pedersen, J.K. Nørskov, Atomic-scale imaging of carbon nanofibre growth. *Nature* **427**(6973), 426–429 (2004). doi:[10.1038/nature02278](https://doi.org/10.1038/nature02278)
118. T.E. Fischer, S.R. Kelemen, Influence of the substrate structure on the bonding of chemisorbed acetylene to transition metal surfaces. *Surf. Sci.* **74**(47), 47–53 (1978). doi:[10.1016/0039-6028\(78\)90270-4](https://doi.org/10.1016/0039-6028(78)90270-4)
119. J. Dvorak, J. Hrbek, Adsorbate ordering effects in the trimerization reaction of acetylene on Cu (100). *J. Phys. Chem. B.* **102**(47), 9443–9450 (1998). doi:[10.1021/jp981956n](https://doi.org/10.1021/jp981956n)
120. J.R. Lomas, C.J. Baddeley, M.S. Tikhov, R.M. Lambert, Ethyne cyclization to benzene over Cu (110). *Langmuir* **11**(8), 3048–3053 (1995). doi:[10.1021/la00008a033](https://doi.org/10.1021/la00008a033)
121. G. Kyriakou, J. Kim, M.S. Tikhov, N. Macleod, R.M. Lambert, Acetylene coupling on Cu (111): formation of butadiene, benzene, and cyclooctatetraene. *J. Phys. Chem. B.* **109**(21), 10952–10956 (2005). doi:[10.1021/jp044213c](https://doi.org/10.1021/jp044213c)
122. W. Alter, D. Borgmann, M. Stadelmann, M. Worn, G. Wedler, Interaction of acetylene with films of the transition-metals iron, nickel, and palladium. *J. Am. Chem. Soc.* **116**(22), 10041–10049 (1994). doi:[10.1021/ja00101a024](https://doi.org/10.1021/ja00101a024)
123. F. Zaera, R.B. Hall, High-resolution electron energy loss spectroscopy and thermal programmed desorption studies of the chemisorption and thermal decomposition of ethylene and acetylene on Ni (100) single-crystal surfaces. *J. Phys. Chem.* **91**(16), 4318–4323 (1987). doi:[10.1021/j100300a023](https://doi.org/10.1021/j100300a023)
124. J.C. Bertolini, J. Massardier, G. Dalmai-Imelik, Evolution of adsorbed species during C₂H₂ adsorption on Ni (111) in relation to their vibrational spectra. *J. Chem. Soc. Faraday Trans. I.* **74**, 1720–1725 (1978). doi:[10.1039/f19787401720](https://doi.org/10.1039/f19787401720)
125. J.A. Stroschio, S.R. Bare, W. Ho, The chemisorption and decomposition of ethylene and acetylene on Ni (110). *Surf. Sci.* **148**(2–3), 499–525 (1984). doi:[10.1016/0039-6028\(84\)90596-x](https://doi.org/10.1016/0039-6028(84)90596-x)
126. A. Benninghoven, P. Beckmann, D. Greifendorf, M. Schemmer, Investigation of surface-reactions by SIMS and TDMS—interaction of ethylene and acetylene with hydrogen on polycrystalline nickel. *Appl. Surf. Sci.* **6**(3–4), 288–296 (1980). doi:[10.1016/0378-5963\(80\)90018-5](https://doi.org/10.1016/0378-5963(80)90018-5)
127. P.M. Mattlis, The oligomerization of acetylenes induced by metals of the nickel triad. *Pure Appl. Chem.* **30**(3–4), 427–448 (1972). doi:[10.1351/pac197230030427](https://doi.org/10.1351/pac197230030427)

128. D.L. Trimm, I.O.Y. Liu, N.W. Cant, The oligomerization of acetylene in hydrogen over Ni/SiO₂ catalysts: product distribution and pathways. *J. Mol. Catal. A Chem.* **288**(1–2), 63–74 (2008). doi:[10.1016/j.molcata.2008.03.022](https://doi.org/10.1016/j.molcata.2008.03.022)
129. B. Lesiak, A. Jablonski, W. Palczewska, I. Kulszewiczbajer, M. Zagorska, Identification of the carbonaceous residues at nickel and platinum surfaces on the basis of the carbon K_{LL} spectra. *Surf. Interf. Anal.* **18**(6), 430–438 (1992). doi:[10.1002/sia.740180610](https://doi.org/10.1002/sia.740180610)
130. S. Hofmann, G. Csanyi, A.C. Ferrari, M.C. Payne, J. Robertson, Surface diffusion: the low activation energy path for nanotube growth. *Phys. Rev. Lett.* **95**(3), 036101 (2005). doi:[10.1103/PhysRevLett.95.036101](https://doi.org/10.1103/PhysRevLett.95.036101)
131. O.V. Yazyev, A. Pasquarello, Effect of metal elements in catalytic growth of carbon nanotubes. *Phys. Rev. Lett.* **100**(15), 4 (2008). doi:[10.1103/PhysRevLett.100.156102](https://doi.org/10.1103/PhysRevLett.100.156102)
132. K. Bartsch, K. Biedermann, T. Gemming, A. Leonhardt, On the diffusion-controlled growth of multiwalled carbon nanotubes. *J. Appl. Phys.* **97**(11), 7 (2005). doi:[10.1063/1.1922067](https://doi.org/10.1063/1.1922067)
133. Z.Y. Juang, J.F. Lai, C.H. Weng, J.H. Lee, H.J. Lai, T.S. Lai, C.H. Tsai, On the kinetics of carbon nanotube growth by thermal CVD method. *Diam. Relat. Mater.* **13**(11–12), 2140–2146 (2004). doi:[10.1016/j.diamond.2004.03.007](https://doi.org/10.1016/j.diamond.2004.03.007)
134. O.A. Louchev, Y. Sato, H. Kanda, Multiwall carbon nanotubes: self-organization and inhibition of step-flow growth kinetics. *J. Appl. Phys.* **89**(6), 3438–3446 (2001). doi:[10.1063/1.1347407](https://doi.org/10.1063/1.1347407)
135. S. Hofmann, B. Kleinsorge, C. Ducati, A.C. Ferrari, J. Robertson, Low-temperature plasma enhanced chemical vapour deposition of carbon nanotubes. *Diam. Relat. Mater.* **13**(4–8), 1171–1176 (2004). doi:[10.1016/j.diamond.2003.11.046](https://doi.org/10.1016/j.diamond.2003.11.046)
136. O.A. Louchev, T. Laude, Y. Sato, H. Kanda, Diffusion-controlled kinetics of carbon nanotube forest growth by chemical vapor deposition. *J. Chem. Phys.* **118**(16), 7622–7634 (2003). doi:[10.1063/1.1562195](https://doi.org/10.1063/1.1562195)
137. O.A. Louchev, Formation mechanism of pentagonal defects and bamboo-like structures in carbon nanotube growth mediated by surface diffusion. *Physica Status Solidi A Appl. Res.* **193**(3), 585–596 (2002). doi:[10.1002/1521-396x\(200210\)193:3<585:aid-pssa585>3.0.co;2-y](https://doi.org/10.1002/1521-396x(200210)193:3<585:aid-pssa585>3.0.co;2-y)
138. O.A. Louchev, Y. Sato, H. Kanda, Growth mechanism of carbon nanotube forests by chemical vapor deposition. *Appl. Phys. Lett.* **80**(15), 2752–2754 (2002). doi:[10.1063/1.1468266](https://doi.org/10.1063/1.1468266)
139. D.C. Li, L.M. Dai, S.M. Huang, A.W.H. Mau, Z.L. Wang, Structure and growth of aligned carbon nanotube films by pyrolysis. *Chem. Phys. Lett.* **316**(5–6), 349–355 (2000). doi:[10.1016/s0009-2614\(99\)01334-2](https://doi.org/10.1016/s0009-2614(99)01334-2)
140. S.A. Dayeh, E.T. Yu, D. Wang, III-V nanowire growth mechanism: V/III ratio and temperature effects. *Nano Lett.* **7**(8), 2486–2490 (2007). doi:[10.1021/nl0712668](https://doi.org/10.1021/nl0712668)
141. P.B. Amama, O. Ogbule, M.R. Maschmann, T.D. Sands, T.S. Fisher, Dendrimer-assisted low-temperature growth of carbon nanotubes by plasma-enhanced chemical vapor deposition. *Chem. Commun.* **27**, 2899–2901 (2006). doi:[10.1039/b602623k](https://doi.org/10.1039/b602623k)
142. H.Y. Wang, J.J. Moore, Low temperature growth mechanisms of vertically aligned carbon nanofibers and nanotubes by radio frequency-plasma enhanced chemical vapor deposition. *Carbon* **50**(3), 1235–1242 (2012). doi:[10.1016/j.carbon.2011.10.041](https://doi.org/10.1016/j.carbon.2011.10.041)
143. S. Hofmann, C. Ducati, J. Robertson, B. Kleinsorge, Low-temperature growth of carbon nanotubes by plasma-enhanced chemical vapor deposition. *Appl. Phys. Lett.* **83**(1), 135–137 (2003). doi:[10.1063/1.1589187](https://doi.org/10.1063/1.1589187)
144. T.M. Minea, S. Point, A. Granier, M. Touzeau, Room temperature synthesis of carbon nanofibers containing nitrogen by plasma-enhanced chemical vapor deposition. *Appl. Phys. Lett.* **85**(7), 1244–1246 (2004). doi:[10.1063/1.1781352](https://doi.org/10.1063/1.1781352)
145. M. Meyyappan, A review of plasma enhanced chemical vapour deposition of carbon nanotubes. *J. Phys. D Appl. Phys.* **42**(21), 15 (2009). doi:[10.1088/0022-3727/42/21/213001](https://doi.org/10.1088/0022-3727/42/21/213001)
146. Y. Ishikawa, K. Ishizuka, Growth of single-walled carbon nanotubes by hot-filament assisted chemical vapor deposition below 500 °C. *Appl. Phys. Express* **2**(4), 3 (2009). doi:[10.1143/apex.2.045001](https://doi.org/10.1143/apex.2.045001)

147. N.G. Shang, Y.Y. Tan, V. Stolojan, P. Papakonstantinou, S.R.P. Silva, High-rate low-temperature growth of vertically aligned carbon nanotubes. *Nanotechnology* **21**(50), 6 (2010). doi:[10.1088/0957-4484/21/50/505604](https://doi.org/10.1088/0957-4484/21/50/505604)
148. Y. Ishikawa, H. Jinbo, Synthesis of multiwalled carbon nanotubes at temperatures below 300 °C by hot-filament assisted chemical vapor deposition. *Jpn. J. Appl. Phys. Part 2 Lett. Express Lett.* **44**(12–15), L394–L397 (2005). doi:[10.1143/jjap.44.L394](https://doi.org/10.1143/jjap.44.L394)
149. Y. Awano, S. Sato, M. Nihei, T. Sakai, Y. Ohno, T. Mizutani, Carbon nanotubes for VLSI: interconnect and transistor applications. *Proc. IEEE* **98**(12), 2015–2031 (2010). doi:[10.1109/JPROC.2010.2068030](https://doi.org/10.1109/JPROC.2010.2068030)
150. C.L. Long, D.P. Qi, T. Wei, J. Yan, L.L. Jiang, Z.J. Fan, Nitrogen-doped carbon networks for high energy density supercapacitors derived from polyaniline coated bacterial cellulose. *Adv. Funct. Mater.* **24**(25), 3953–3961 (2014). doi:[10.1002/adfm.201304269](https://doi.org/10.1002/adfm.201304269)
151. N.P. Wickramaratne, J.T. Xu, M. Wang, L. Zhu, L.M. Dai, M. Jaroniec, Nitrogen enriched porous carbon spheres: attractive materials for supercapacitor electrodes and CO₂ adsorption. *Chem. Mater.* **26**(9), 2820–2828 (2014). doi:[10.1021/cm5001895](https://doi.org/10.1021/cm5001895)
152. W. Wei, H.W. Liang, K. Parvez, X.D. Zhuang, X.L. Feng, K. Mullen, Nitrogen-doped carbon nanosheets with size-defined mesopores as highly efficient metal-free catalyst for the oxygen reduction reaction. *Angewandte Chemie-International Edition* **53**(6), 1570–1574 (2014). doi:[10.1002/anie.201307319](https://doi.org/10.1002/anie.201307319)

Carbon Nanoparticles and Nanostructures

Yang, N.; Jiang, X.; Pang, D.-W. (Eds.)

2016, VII, 356 p. 156 illus., 93 illus. in color., Hardcover

ISBN: 978-3-319-28780-5